Title

Late-life dietary folate restriction reduces biosynthetic processes without compromising healthspan in mice

Authors

Heidi M. Blank[1], Staci E. Hammer[1], Laurel Boatright[1,2], Courtney Roberts[1], Katarina E. Heyden[3], Aravindh Nagarajan[2,4], Mitsuhiro Tsuchiya[5], Marcel Brun[6], Charles D. Johnson[6], Patrick J. Stover[1,7,13], Raquel Sitcheran[8], Brian K. Kennedy[9,10], L. Garry Adams[11], Matt Kaeberlein[5,12], Martha S. Field[3], David W. Threadgill[1,4,13,14], Helene L. Andrews-Polymenis[2,4], Michael Polymenis[1,4,7]

Affiliations

[1]Department of Biochemistry and Biophysics, Texas A&M University, College Station, United States.

[2]Department of Microbial Pathogenesis and Immunology, School of Medicine, Texas A&M University Health Science Center, Bryan, United States.

[3]Division of Nutritional Sciences, Cornell University, Ithaca, United States.

[4]Interdisciplinary Program in Genetics, Texas A&M University, College Station, United States.

[5]Department of Laboratory Medicine and Pathology, University of Washington, Seattle, United States.

[6]Texas A&M Agrilife Research, Genomics and Bioinformatics Service, College Station, United States.

[7]Institute for Advancing Health through Agriculture, Texas A&M University, College Station, United States.

[8]Department of Cell Biology and Genetics, School of Medicine, Texas A&M University Health Science Center, Bryan, United States.

[9]Departments of Biochemistry and Physiology, Yong Loo Lin School of Medicine, National University of Singapore, Singapore, Singapore.

[10]Centre for Healthy Ageing, National University of Singapore, National University Health System, Singapore, Singapore.

[11]Department of Veterinary Pathobiology, College of Veterinary Medicine, Texas A&M, College Station, Texas, USA.

[12]Optispan, Inc., Seattle, United States.

[13]Department of Nutrition, Texas A&M University, College Station, United States.

[14]Texas A&M Institute for Genome Sciences and Society, Texas A&M University, College Station, United States.

Contact

Michael Polymenis (michael.polymenis@ag.tamu.edu)

ABSTRACT

Folate is a vitamin required for cell growth and is present in fortified foods in the form of folic acid to prevent congenital abnormalities. The impact of low folate status on life-long health is poorly understood. We found that limiting folate levels with the folate antagonist methotrexate increased the lifespan of yeast and worms. We then restricted folate intake in aged mice and measured various health metrics, metabolites, and gene expression signatures. Limiting folate intake decreased anabolic biosynthetic processes in mice and enhanced metabolic plasticity. Despite reduced serum folate levels in mice with limited folic acid intake, these animals maintained their weight and adiposity late in life, and we did not observe adverse health outcomes. These results argue that the effectiveness of folate dietary interventions may vary depending on an individual's age and sex. A higher folate intake is advantageous during the early stages of life to support cell divisions needed for proper development. However, a lower folate intake later in life may result in healthier aging.

INTRODUCTION

Folate is a metabolic cofactor that transfers single-carbon functional groups (one-carbon units; 1C; see Figure 1A) within a metabolic network known as folate-mediated one-carbon metabolism (FOCM). These reactions are involved in the metabolism of amino acids (primarily Ser, Gly, Met, and His), the synthesis of purines, thymidylate, and phospholipids and numerous methylation reactions (Ducker and Rabinowitz, 2017; Fox and Stover, 2008; Labuschagne et al., 2014; Locasale, 2013; Reina-Campos et al., 2019; Rosenzweig et al., 2018; West et al., 1996; Zheng and Cantley, 2019). Hence, folate is vital for cell division, especially during rapid proliferation states, including fetal development. Conversely, antifolate drugs have been used for decades to inhibit excessive cell proliferation in cancer, rheumatoid arthritis, and psoriasis. To help prevent congenital disabilities, the US and other countries have implemented large-scale folate fortification of staple foods. The benefits of dietary folate early in life are well-studied and documented. In contrast, its role later in life in modulating the healthy, disease-free period of an individual's life (a.k.a. healthspan) is poorly understood.

Concerns have been raised that mandatory folic acid fortification could negatively affect older individuals. Some observations suggested a possible link between folic acid fortification and increased colorectal cancer rates in the 1990s (Mason et al., 2007). However, later analyses "did not identify specific risks from existing mandatory folic acid fortification" in the general population (Field and Stover, 2018). This conclusion neither refutes nor contradicts the idea that a moderate decrease in folic acid intake among older adults may improve healthspan. Merely because high folic acid intake does not harm the health of older adults does not negate the possibility that a lower folic acid intake might enhance health.

Previous work from several labs, including ours (Maitra et al., 2020), suggested that loss-of-function genetic interventions in 1C enzymes promote longevity in invertebrate model

systems. Lower methyl-tetrahydrofolate (methyl-THF) level is a common signature of pro-longevity pathways (Annibal et al., 2021), and methionine restriction extends longevity in several organisms (Barcena et al., 2018; Johnson and Johnson, 2014; Kozieł et al., 2014; Lee et al., 2016, 2014; Miller et al., 2005; Orentreich et al., 1993; Ruckenstuhl et al., 2014; Sun et al., 2009; Zou et al., 2020). Mutations in the large (60S) subunit ribosomal proteins constitute a significant class of pro-longevity mutations in yeast and other species (Hansen et al., 2007; Kaeberlein et al., 2005; Kaeberlein and Kennedy, 2011; McCormick et al., 2015; Steffen et al., 2012, 2008). Using ribosome profiling, we identified translational control patterns responsible for increased longevity. Long-lived mutants had significantly reduced translational efficiency of transcripts encoding enzymes of the broader network of 1C metabolism (Maitra et al., 2020). Steady-state metabolite profiling of these mutants was consistent with changes in 1C metabolism (Maitra et al., 2020).

The effects of folate intake in aged adults have yet to be studied in mouse models, where causal mechanisms can be examined more precisely. In this report, we examined healthspan as a function of dietary folate intake in the long-lived inbred mouse strain C57BL/6J. We found that restricting folate intake in aged mice does not adversely affect their health and may even improve their metabolic plasticity, as they switch between glycolysis and oxidative phosphorylation states during their regular diurnal cycles. Metabolite changes in the folate-restricted animals suggest reduced anabolism. Similarly, the abundance of transcripts encoding gene products involved in protein synthesis was reduced in animals limited for folate late in life. These results are consistent with a view of 1C metabolism as a tunable platform that allocates cellular resources for biosynthesis. They also suggest that the outcomes of folate dietary interventions might depend on an individual's age. Adequate folate status is required during development for neural tube closure. Late in life, a lower folate intake might promote healthy aging.

RESULTS

Inhibitors of 1C metabolic enzymes extend the lifespan of yeast and worms

We reasoned that if genetic interventions of 1C metabolism extend yeast's lifespan, chemical ones may also. Methotrexate leads to tetrahydrofolate (THF) limitation (Rajagopalan et al., 2002). Methotrexate has been used extensively since its introduction in the 1950s but has not been evaluated for longevity effects. We found that methotrexate (at 0.5-10μM) increased yeast replicative lifespan (Figure 1B, $p<0.05$ based on the log-rank test). The dose with the maximal (~15%) lifespan extension was 1μM (Figure 1B). At such low doses, methotrexate did not affect cell proliferation significantly (not shown). We also looked at cell size as a proxy of cell cycle effects. Folate deficiencies and drugs that interfere with DNA replication are often associated with increased cell size, leading to megaloblastosis (Das et al., 2005; Scott and Weir, 1980). Because methotrexate inhibits dihydrofolate reductase (DHFR), it limits the levels of THF for thymidylate synthesis and DNA replication (Rajagopalan et al., 2002). At concentrations up to 10μM, methotrexate increased cell size slightly (from 47fL to 52fL; Figure 1 - Supplement 1). At higher concentrations, methotrexate did not extend replicative longevity (Figure 1B) and increased cell size more significantly (from 47fL to 56-64fL, for 50-100μM, respectively; Figure 1 - Supplement 1), indicating a stronger cell cycle block. These data are consistent with the notion that moderate, but not severe, cell cycle delays are associated with longer replicative lifespan in yeast (He et al., 2014).

Given the conservation of 1C pathways, we asked if methotrexate could increase the lifespan of wild-type *C. elegans* animals. It has been reported that folate accelerates worm aging, but treating worms with methotrexate at the adult stage did not extend their lifespan (Virk et al., 2016). Because adult worms are post-mitotic, we exposed *C. elegans* to the drug continuously, from the embryo stage until death (Figure 1C). Worms exposed to low doses of methotrexate (1-3μM) had a longer lifespan (~15% lifespan extension, $p<2E-14$ based on the

log-rank test, Figure 1C). The bacteria used to feed the worms in these experiments were killed by ultraviolet radiation to exclude any effects due to altered bacterial proliferation. We conclude that the longevity extension by methotrexate is conserved between yeast and invertebrates.

To further test the generality of the idea that 1C interventions promote longevity, we examined another commercially available inhibitor of a 1C enzyme. A dipeptide that blocks the requisite dimerization of ATIC (AICAR Transformylase/Inosine Monophosphate Cyclohydrolase; see Figure 1A) has been previously shown to activate the AMPK signaling pathway and ameliorate the metabolic syndrome in mice (Asby et al., 2015). In experiment-matched assays, the ATIC inhibitor also increased the lifespan of worms (Figure 1D) at 100μM, a dose similar to the one used in mice with metabolic syndrome (Asby et al., 2015).

To our knowledge, the above is the first evidence arguing that pharmacologic interventions of 1C metabolism increase the lifespan of invertebrate model organisms, raising the exciting possibility that 1C interventions may improve longevity in mammals. Acute toxicity of methotrexate was measured in numerous studies, starting in 1950 with measurements in mice, rats, and dogs (Ferguson et al., 1950; Philips et al., 1950). Only later, in the 1970s, rodents were subjected to low-dose, long-term treatment with methotrexate to measure its toxicity (Freeman-Narrod and Narrod, 1977; Rustia and Shubik, 1973). Methotrexate given to 7-week-old Syrian hamsters for several months was tolerated well at 5, 10, and 20ppm (Rustia and Shubik, 1973). Methotrexate was also tolerated quite well in mice when administered at 3, 5, 8, or 10ppm in the diet (Rustia and Shubik, 1973) or by IP injection at 0.25-2mg/kg (Freeman-Narrod and Narrod, 1977). We reasoned that those long-term studies might offer helpful information about the role of folate limitation in longevity in mice. We generated survival curves from the available historical data (0-10ppm MTX) given in alternating weeks in the diet in male and female Swiss mice from 7 to 120 weeks of age. In 5 of the 8 conditions tested, the mean lifespan was longer than in the control group. In one case, it was significantly so ($p=0.04$,

based on the log-rank test, Figure 1 - Supplement 2). The number of females used was too low to detect significant differences in lifespan and no healthspan parameters were evaluated in those studies (Rustia and Shubik, 1973). These limitations notwithstanding, the results are remarkable because the drug was administered from a young age (7 weeks) when side effects are strikingly more pronounced. The LD50 for methotrexate given to 5-week-old mice is 59mg/kg, whereas that for 16-week-old mice is 284mg/kg (Freeman-Narrod and Narrod, 1977). Based on these observations, and our results in yeast and worms (Figure 1) we decided to measure if folate limitation later in life improves healthspan in mice.

Mice placed under dietary folate restriction late in life maintain or increase their weight and do not develop anemia

Since relatively little is known about healthspan as a function of dietary folate intake, we designed a study in the long-lived inbred strain C57BL/6J (Figure 2A, and Materials and Methods). Longevity was not the measured outcome; the mice were sacrificed at 120 weeks. However, with a sample size of 20 mice per group, there was sufficient power to detect significant ($p<0.05$ and 80% power) differences (1SD) in healthspan parameters (Bellantuono et al., 2020). Starting at 52 weeks of age, half the mice were maintained on the standard diet (AIN-93M; (Reeves et al., 1993)), and the other half were placed on a folate/choline-deficient (F/C-) diet. Before the diet changes at 52 weeks of age, the mice were randomly assigned to the different test groups based on their lean mass. The standard diet contains 2mg/kg of folic acid and 2.5g/kg choline bitartrate (F/C+), while the F/C- diet contains 0mg/kg of folic acid and 0mg/kg choline bitartrate. As expected, serum folate levels were greatly reduced in the F/C- groups ($p=0.00216$ for the females and $p=0.00012$ for the males, based on the Wilcoxon rank sum test; Figure 2B).

In people, folate supplementation during pregnancy is positively associated with birth weight (Scholl and Johnson, 2000), but in older adults there is no association between folate status and weight (Soysal et al., 2019). We found that the weight of mice from either sex was not reduced from 52 weeks of age when placed on the F/C- diet until the end of the study at 120 weeks of age (Figure 1C). Instead, male mice on the F/C- diet appeared to gain weight (Figure 1C, compare the two left panels). To evaluate the statistical significance of this observation, we applied a mixed effects regression model to analyze the repeated longitudinal weight measurements using the lme4 and lmer R language packages. The model was valid because from a scatter plot of the standardized residuals vs. the fitted values, the residuals were symmetrically distributed around zero, with approximately constant variance (Figure 2 - Supplement 1A). Furthermore, the normality of the residuals was checked with a quantile-quantile plot (Figure 2 - Supplement 1B). Based on the mixed effects regression model, there was a negative effect between diet (F/C+) and weight (slope=-1.96, p=0.0313). As expected, there was a small but significant positive relation between weight and time (slope=0.075, p<2E-16) and a strong one between weight and male sex (slope=7.72, p=6.48E-13).

The mice on the F/C- diet were not anemic (Figure 2 - Supplement 2). They had the same blood cell counts as the mice on the F/C+ diet (Figure 2 - Supplement 2A). There were also no cell size changes or evidence of megaloblastosis (Figure 2 - Supplement 2B), which one might expect if DNA replication in erythrocytes was significantly inhibited (Das et al., 2005). Lastly, mice on the F/C- diet did not have reduced survival compared to animals of the same sex that were kept on the F/C+ diet (Figure 2 - Supplement 3). It is unclear why the female animals had reduced survival compared to males. Still, the increased mortality of C57BL/6J females is in line with data from the Aged Rodent Colonies maintained by the National Institute on Aging. Females experience 50-66% mortality between 20 and 30 months of age vs. 30-36% mortality

for male mice (Turturro et al., 1999). These data show that dietary folate limitation late in life does not lead to anemia, reduced viability, or reduced body weight. In contrast, at least in the case of males, folate-limited animals have a slightly higher body weight.

No adverse healthspan metrics in mice placed on dietary folate restriction late in life

At the indicated times shown in Figure 2A, we evaluate various metrics associated with healthspan. Mice on the F/C- diet had similar Frailty Index scores ($p=0.434$, based on a mixed effects regression model) with their counterparts on the F/C+ diet (Figure 3A). The Frailty Index is a clinically validated metric comprising several visible clinical signs of physical deterioration, as previously described for aging C57BL/6J mice (Kane et al., 2016; Whitehead et al., 2014). Note that at the "<52w" timepoint, the diet had not been switched yet, and all the mice were on the F/C+ diet. However, to accurately track individual animals and visualize the data, the mice that were placed in the different diet groups at 52 weeks of age are also depicted in the same groups at the "<52w" time point.

In addition to the regular body weight measurements described in Figure 2, we also evaluated body composition based on measurements with EchoMRI (Figure 3B). There was again a significant negative effect from the F/C+ diet on total body mass (slope=-2.1674, $p=0.04580$, based on a mixed effects regression model). There was also a similar negative trend between the F/C+ diet and fat mass (slope=-1.6989, $p=0.0635$), and a weaker negative association with lean mass (slope=-0.5034, $p=0.1474$), although in the latter cases the effects did not reach the $p<0.05$ threshold. Overall, we conclude that the increased weight of the mice on the folate-limited diet late in life is roughly proportional, but likely with a greater contribution from a gain of fat vs. lean mass.

Regarding the other healthspan-related metrics we evaluated at 68, 94, and 120 weeks of age (see Figure 2A and Materials and Methods), there were no significant diet effects based

on mixed effects models. The metrics we measured included gait analysis during voluntary walking, which evaluates a wide range of ambulatory problems, using the accurate and high throughput DigiGait system (Figure 3 - Supplement 1), open field (Figure 3 - Supplement 2A), and novel object recognition (NOR) parameters (Figure 3 - Supplement 2B), which evaluate cognitive behavior and memory. In the case of NOR, in addition to the discrimination index (DI) values shown in Figure 3 - Supplement 2B, we also evaluated differences in a binary, pass-fail format. We chose a DI>0.06 as the cutoff for a passing novel object test, as this also correlated visually with what was seen on a heat map of exploration around each object. Based on χ^2 tests, there were again no significant diet effects. Lastly, cardiac function was evaluated with echocardiography using the Vevo 3100 Ultrasound device, looking specifically for aging-related changes in cardiac physiology (Lindsey et al., 2018). Cardiac output, systole and diastole diameter, ejection fraction, and fractional shortening were all unaffected by diet (Figure 3 - Supplement 3).

Metabolic activity of aged mice on the folate-restricted diet

Not only were no healthspan metrics adversely affected by limiting dietary folate intake late in life (Figure 3), but we also noticed some possible positive outcomes. At ~85 weeks of age, the male animals on the folate-limited diet were visibly less gray than their counterparts on the folate-replete diet (Figure 4A). Although graying is not necessarily associated with declining health, it is usually an age-dependent trait. Notably, recent work in human cells showed that inhibiting the target of rapamycin (TOR) inhibits graying (Suzuki et al., 2023), consistent with the idea that delayed hair graying may be an outcome of interventions that improve healthspan.

Since folate-based 1C chemical reactions are a metabolic hub (see Figure 1A), we placed individual animals in TSE Phenomaster metabolic cages (see Materials and Methods). We measured several physiological parameters reporting global metabolic features (Figure 4B). A metric of particular significance is the respiratory exchange ratio (RER), which is the ratio

between the metabolic production of carbon dioxide (CO_2) and the uptake of oxygen (O_2). RER is an indicator of whether carbohydrate or fat is being metabolized. An RER <1 suggests that fat is predominantly used (e.g., during sleep). A value of 1 is indicative of carbohydrate use. RER can exceed 1 during exercise. How fast the RER changes between periods of inactivity vs. activity (e.g., during diurnal transitions) reflects metabolic plasticity, which is expected to decline with age. Male animals on the F/C+ diet increased their RER as they became more active during the night (Figure 4B, left bottom panel). The rise in the RER was markedly slower in the female animals on the F/C+ diet (Figure 4B, left top panel), suggesting reduced metabolic plasticity. Their counterparts on the F/C- diet maintained metabolic plasticity, transitioning much faster to carbohydrate-based fuel consumption (Figure 4B, compare the two top panels). Furthermore, the male mice on the F/C- diet had slightly higher RER values at night than those on the F/C+ diet (Figure 4B, compare the two bottom panels). Based on mixed effects regression models for the period during the transition from daytime to night (time 700-1100 min in Figure 4B), the effects of time and sex (males) on the RER increase were positive and significant (p=1E-06 and p=0.0101, respectively), while there was a negative association with the F/C+ diet (p=0.0806). These data suggest that a late-life folate-limited diet might have metabolic benefits, albeit for different reasons in the two sexes. Female mice appeared to have improved metabolic plasticity, while males reached higher RER values.

Changes in the intestinal microbiome of mice limited for folate late in life

Since the microbiome likely contributes to 1C metabolism, we sampled and sequenced the DNA of the fecal microbiome at 90 weeks of age. The analysis yielded standard diversity metrics to assess differences in the fecal microbiome's makeup among the mice groups (Figure 5). The different sex and diet groups had an easily distinguishable gut microbiome (Figure 5A) based on Bray-Curtis β-diversity dissimilarity indices (Knight et al., 2018). The intestinal microbiome of

male mice on the F/C- diet appeared less diverse (Figure 5 - Supplement 1), but the difference was not statistically significant (p=0.222, based on the Wilcoxon rank sum test).

We looked at biomarkers from the same metagenomic datasets to place the above differences in the context of 1C metabolism. The LEfSe computational pipeline was used to determine the features most likely to explain the observed differences (Segata et al., 2011). Notably, the LEfSe algorithm incorporates effect sizes, ranking the relevance of the identified biomarkers and enabling their visualization through the computed linear discriminant analysis (LDA) scores (Segata et al., 2011). We found that the microbiome pathway changes were essentially dimorphic for sex. Only an enrichment for Coenzyme A biosynthesis was evident in male and female mice on the folate-replete diet (Figure 5B, bottom bar). All other changes were from one sex (to simplify the visualization, we grouped the data from both sexes). Overall, pathways involved in amino acid (Figure 5B; black arrows) and IMP (Figure 5B; gray arrows) synthesis were enriched in mice on the folate-limited diet. These data suggest that under dietary folate limitation, the microbiome may be a source of metabolites that are known outputs of 1C metabolism (e.g., methionine, and IMP, from which all purine nucleotides are made).

Metabolite and gene expression changes in the folate-restricted animals consistent with a reduced anabolism

To gauge immune function, we measured the levels of 32 serum cytokines at the time of euthanasia, at 120 weeks of age (Figure 6 - Supplement 2). The differences were again minimal, and those that passed the $p<0.05$ threshold (indicated with the red asterisks in Figure 6 - Supplement 2) probably were due to lower variance in the measured values and not to major changes in the levels of those cytokines, comparing animals of the same sex but on different diets. These apparent changes, based on the Wilcoxon rank sum test, were: lower IL-15 levels

in females on the F/C- diet (p=0.0426); higher IL-17 levels in females on the F/C- diet (p=0.0127); lower VEGF levels in females on the F/C- diet (p=0.0237); and higher LIX levels in males on the F/C- diet (p=0.0015).

Pathologic evaluation of various organs of the euthanized animals at 120 weeks of age revealed minimal effects on overall disease burden, other than an apparent increase in kidney abnormalities in male animals on the F/C- diet (Figure 6 - Supplement 1). Nearly all the mice had some degree/number of perivascular lymphoplasmacytic nodules (Russell bodies), frequently with immunoglobulin aggregates in the ER of plasma cells in the spleen, liver, kidney, and lung. These nodules tended to be higher in number and larger (although only significant in male kidneys) in mice on the F/C- diet, particularly females. This lesion is compatible with but not diagnostic for autoimmune diseases such as Systemic Lupus Erythematosus in aging women. We note, however, that although the levels of the pro-inflammatory IL-17 were elevated in female mice as well, no leukocytosis was detected.

We next measured signatures associated with genomic instability. Based on targeted bisulfite sequencing at ~2000 loci, there were no changes in the DNA methylation levels from liver samples collected at 120 weeks of age (Figure 6 - Supplement 3A). This analysis yielded an estimate of the DNA methylation age (shown on the y-axis in Figure 6 - Supplement 3A), which was not different among the sexes and diet groups. The negative values in all groups we examined reflect comparisons with the expected standard values for the strain C57BL/6J and liver tissue we examined, making all our groups appear “younger” than expected for unknown reasons. These data suggest that limiting folate late in life did not lead to significant epigenetic changes. We also found that uracil misincorporation was not significantly elevated in liver samples collected at 120 weeks of age from mice on the F/C- diet (Figure 6 - Supplement 3B). Uracil misincorporation into the genome may reflect limited folate availability for DNA synthesis (i.e., if folate is available, then thymidylate synthesis is unperturbed, and little uracil is expected

to be incorporated into the DNA). Hence, limiting folate late in life does not appear to lead to genomic instability in mouse liver, though uracil levels are known to vary by tissue in other systems of folate limitation (Chon et al., 2019).

We next sought to identify broad molecular pathway changes associated with folate restriction late in life. First, we measured amino acid levels in the sera of all remaining animals, before they were euthanized. Serum glutamine levels were markedly elevated (~3-fold) in male mice on the folate-limited diet (Figure 6A). We did not observe any other significant changes in serum amino acid levels.

Second, we measured the levels of ~600 metabolites from liver samples of all mice that were alive at 120 weeks of age by mass spectrometry. In male animals, the metabolite with the lowest relative abundance in folate-limited animals was IMP. Serine had the highest relative abundance (Figure 6B). These results are consistent with reduced 1C metabolism because serine is the primary 1C input (Figure 1A). The purine nucleotide IMP is a major output (Figure 1A). Among 589 metabolites detected and assigned, we looked for pathway enrichment with the MetaboAnalyst platform (Chong et al., 2019). There were no significantly overrepresented pathways in either male or female folate-limited animals. In females, pyrimidine metabolism may be under-represented ($p=0.00103$, FDR=0.101). In males, metabolites associated with the pentose phosphate pathway, methionine metabolism, and Warburg effect pathways were significantly underrepresented in mice on the F/C- diet (Figure 6C). These results fit a view of 1C metabolism as a platform that primarily allocates resources for anabolic, biosynthetic pathways. Reducing the output of these pathways late in life is known to promote longevity in other settings.

Third, to gauge if and how a folate-limited diet late in life impacts gene expression, we measured transcript steady-state levels of liver tissue with RNAseq. We did not see extensive

transcriptome remodeling in response to the folate-limited diet (Figure 7). Less than 5% of the 15,000-20,000 transcripts that entered the analysis changed in abundance significantly (>1.5-fold, $p<0.05$; see Materials and Methods and Figure 7A). Among the transcripts over-expressed in mice on the F/C- diet, there was no significant enrichment of any gene ontology biological process. On the other hand, among under-expressed transcripts, we found significant enrichment of transcripts encoding gene products involved in protein synthesis in both male (Figure 7B) and female animals (Figure 7C). The enrichment was stronger in males (>3-fold) than in females (~2-3-fold) but significant in both sexes (FDR<0.05). These results agree with our metabolite analyses (see Figure 6C), arguing again that a folate-limited diet late in life induces a state of lower anabolism. As a rough readout of proliferative signaling, we next looked at the levels of phosphorylation of ribosomal protein S6 (RPS6), which is an output of several kinase cascades, including the mTOR pathway (Meyuhas, 2015; Wu et al., 2022). The values detected by immunoblots from liver tissue samples collected at euthanasia varied among the mice. Although male animals on the folate-limited diet as a group had about half the levels of phosphorylated RPS6 than their counterparts on the folate-replete diet, there was an animal on the F/C- diet with very high levels of P-RPS6 and the overall differences were not statistically significant (Figure 7 - Supplement 1; $p>0.05$, based on the Wilcoxon rank sum test).

Lastly, we also measured IGF-1 levels in the sera of all animals at the endpoint of euthanasia using an ELISA-based assay (see Materials and Methods). The insulin/insulin-like growth factor pathway plays critical roles in growth control and longevity, mirroring the effects of the mTOR pathway. We found that female mice on the folate-limited diet had ~40% lower IGF-1 levels than their counterparts on the folate-replete diet (Figure 7 - Supplement 2; $p=0.028$, based on the Wilcoxon rank sum test). These data are again consistent with the notion that a folate-limited diet late in life may induce a state of lower cell growth and anabolism.

DISCUSSION

The results provide important insights into how adjusting folate intake in older adults may promote health at this later stage of life. Our data raise the exciting possibility that the amount of folate needed to promote health changes at different stages of life and that reduced folate intake later in life might be beneficial.

What theoretical framework explains the proposed differential impacts of folate consumption during different stages of life? Antagonistic pleiotropy offers insight into these age-specific effects, suggesting that early-life advantages in fitness and reproduction come at a cost later (Williams, 1957). This theory, introduced by Williams in the ’50s, proposes that “an individual cannot be exceptionally gifted with both youthful vigor and long life” (Williams, 1957). Antagonistic pleiotropy is now widely acknowledged in aging biology (Austad and Hoffman, 2018; Promislow, 2004), with the “target of rapamycin” (TOR) pathway serving as a cardinal example (Blagosklonny, 2010).

Folate pathways and their role in healthspan may be analogous to the TOR pathway. 1C metabolism allocates resources for biosynthesis, providing precursors for nucleotides, proteins, and lipids (Figure 1A). 1C metabolism also adjusts the methylation and redox status of the cell (Ducker and Rabinowitz, 2017; Reina-Campos et al., 2019; Rosenzweig et al., 2018). 1C pathways are uniquely positioned to affect several established hallmarks of aging (Lopez-Otin et al., 2013). TOR orchestrates translation and various metabolic reactions, including 1C reactions (Ben-Sahra et al., 2016), to promote cell growth and proliferation (Barbet et al., 1996). Inhibiting the TOR pathway genetically or chemically inhibits cell division (Barbet et al., 1996) but promotes longevity (Johnson et al., 2013). Notably, such differential effects, predicted by antagonistic pleiotropy, could make folate interventions in aged individuals feasible and effective

without impeding the benefits of high folate intake during early life.

Despite the evidence we outlined above from model organisms, is folate limitation even compatible with improved longevity in people? Genetic evidence supports this idea. Methylenetetrahydrofolate reductase (MTHFR) converts CH_2-THF to methyl-THF (see Figure 1A). A C677T mutation, leading to an Ala to Val substitution in the MTHFR gene, lowering this enzyme's activity by about half. Among French centenarians and nonagenarians with a family history of longevity, the prevalence of the MTHFR C677T allele was higher than in controls (<70 years of age), approaching statistical significance (p=0.06), and C677T carriers had extremely low-folate serum levels (Faure-Delanef et al., 1997). These observations suggest that individuals with lower serum folate levels *can* undoubtedly live longer.

Most animals, including humans, cannot synthesize folate. Folate and its various forms, including 5-methyltetrahydrofolate, the naturally occurring form absorbed through the intestinal mucosa, do not cross biological membranes. Hence, cells rely on receptors or transporters that bind folate and bring it inside cells. Dietary folate is absorbed primarily in the duodenum by the proton-coupled folate transporter (PCFT/SLC46A1) (Qiu et al., 2006; Visentin et al., 2014). Mice with a homozygous deletion of the *Pcft* gene have defective erythropoiesis and fail to thrive, resembling the hereditary folate malabsorption syndrome in humans (Salojin et al., 2011). The heterozygous *Pcft*$^{+/-}$ mice have significantly reduced (~50%) folate levels in serum, liver, kidney, and spleen (Salojin et al., 2011). Remarkably, however, erythropoiesis, growth rate, and survival of these *Pcft*$^{+/-}$ animals were indistinguishable from their wild type counterparts (Salojin et al., 2011).

How could a folate-limited diet late in life improve healthspan? Our metabolomic and transcriptomic profiling experiments likely offer a possible and relatively straightforward answer, revealing signatures of downregulated cellular anabolic processes in the folate-limited animals. Reduced anabolism is common among pro-longevity interventions, for example, when inhibiting

the master regulator of cell growth, the TOR pathway (Johnson et al., 2013). We note that a down-regulation of anabolic signatures in the folate-limited animals was evident in both sexes (Figure 7), arguing that the changes we observed reflect broad and common outcomes of folate limitation. Another signature we observed, at least in males, was elevated serum glutamine levels (Figure 6A). In human studies, centenarians have elevated serum glutamine compared to 70-year-olds (Montoliu et al., 2014). Furthermore, glutamine supplementation in elderly subjects may improve inflammatory responses, redox balance, and exercise performance (Almeida et al., 2020). In contrast, low serum glutamine levels are associated with increased morbidity and mortality (Boelens et al., 2001), but it is unclear if and how the markedly elevated glutamine levels we observed promote longevity.

On the other hand, at least in model organisms, lowering the output of the IGF-1 pathway is known to promote longevity, and it was the first pathway shown to extend lifespan (Kenyon, 2011). Heterozygous female mice carrying a knockout allele of the IGF-1 receptor have ~30% longer lifespan (Holzenberger et al., 2003). Reduced serum levels of IGF-1 are associated with longer lifespan among a panel of inbred strains of mice (Yuan et al., 2009). The effects of IGF-1 signaling in people may also be a manifestation of antagonistic pleiotropy, with low levels being harmful early but beneficial later in life (Zhang et al., 2021). In this context, the lower IGF-1 levels we observed in female mice on the folate-limited diet may be consistent with possible positive outcomes on longevity.

Lastly, we note that male and female mice on the folate-limited diet maintained their weight better as they aged than their counterparts on the folate-replete diet (Figure 2), likely through increased adiposity. A recent study identified these phenotypes as top predictors for positive effects on health and lifespan in genetically diverse mice on various dietary restriction diets (Di Francesco, A. et al., 2023).

Although our mouse study suggests that restricting folate intake late in life is not harmful

and may even be beneficial, we caution that there are significant limitations. For example, our data was from one inbred mouse strain and a relatively small sample size. Similar experiments in larger, genetically diverse populations are better suited for studying genome-by-diet interactions. While exposure to the F/C- diet did not increase liver uracil DNA content, it is possible that more proliferative tissues, such as the colon, are more susceptible to decreased dietary folate availability (Chon et al., 2019). Moreover, our microbiome data (Figure 5) were limited in scope, relying exclusively on metagenomic pieces of evidence. The intestinal microbiome likely represents a significant source of folate and 1C metabolites. To properly investigate diet-host-microbiome relations, combining metagenomic and transcriptomic queries of the microbiome would be needed at various time points during the folate-related dietary interventions. Such approaches could more precisely identify which microbial species are present in what proportions and which microbial processes are critical in the responses to dietary folate limitation.

Despite the above limitations, the experiments we described may have important implications for public health because the US and many other countries mandate folate fortification of staple foods to harness the known benefits of folate supplementation during pregnancy and early stages of life. However, such policies affect people of all ages, and the impact of folate intake on broad healthspan parameters later in life is relatively unexplored. Lastly, that a folate-restricted diet likely leads to a less anabolic state offers new pharmacologic avenues to promote such a state, with known pro-longevity outcomes. Over the last several decades, many drugs have targeted folate-based metabolism, which could be further explored in longevity interventions.

MATERIALS AND METHODS

Materials and resources are listed on the Key Resources Table.

Replicative lifespan assays and cell size measurements in yeast

All the assays were done in the standard *S. cerevisiae* strain BY4742 (MATα *his3Δ1 leu2Δ0 lys2Δ0 ura3Δ0*) on solid rich undefined media (YPD; 1% $^{w}/_{v}$ yeast extract, 2% $^{w}/_{v}$ peptone, 2% $^{w}/_{v}$ dextrose, 2% $^{w}/_{v}$ agar), as described previously (Steffen et al., 2009). Methotrexate was dissolved in dimethylsulfoxide (DMSO) and used at the final concentrations shown in Figure 1B-D. The cell size measurements shown in Figure 1 - Supplement 1 were also done in strain BY4742 in YPD. Briefly, overnight cultures were diluted to ~5E+05 cells/mL in fresh media, allowed to proliferate for 2-3h at 30°C, and then methotrexate was added at the indicated final concentrations. 4-5h later, cell size was measured with a Z2 Channelyzer, as described previously (Soma et al., 2014).

Lifespan assays in worms

All the assays were done at 20°C using *C. elegans* strain N2 and a bacterial strain (OP50) commonly used as food for the worms, as described previously (Sutphin and Kaeberlein, 2009).

Animals

One cohort of female and male C57BL6/J mice, comprising 40 animals per sex, were purchased from Jackson Laboratories at 28 weeks of age. All mice were housed on a 12-hour light/dark cycle and kept at 20–22°C. Until 52 weeks of age, all animals were fed the standard purified diet AIN-93M (Reeves et al., 1993), referred to as F/C+ throughout the text. At 52 weeks of age, half

the animals were switched to a modified AIN-93M diet lacking folate and choline, referred to as F/C- throughout the text until the termination of the study. Both diets were from Dyets Inc. (Bethlehem, PA); see Key Resources Table.

Mice were housed in groups of no more than 5 animals per cage at the TAMU Comparative Medicine Program (CMP) facilities. There was no incident of aggressive males needing to be isolated to prevent fighting. All the animals were scored for various phenotypic metrics (see Figure 2A) at 42 weeks of age before grouping into the different diets. Grouping was randomized based on lean mass values. In addition, partitioning into the two diet groups was balanced for all other metrics we evaluated so that for any given mouse in any given group, there were similar mice in the other diet group of the same sex.

The animals were inspected daily and treated for non-life-threatening conditions as directed by the veterinary staff of TAMU-CMP. The only treatment received was for dermatitis (topical solution thrice weekly, as needed). Each room contained sentinel animals housed in filtered cages. When cages were scheduled to be changed, a small amount of dirty bedding was collected from a (rotated) selected rack of cages and added to the fresh sentinel cage to ensure that the sentinel animals were uniformly exposed to any contaminant or pathogen that may be present within the colony. One sentinel animal from each group was sampled quarterly, and the serum was tested for common rodent pathogens. A veterinary pathologist performed microbiology, parasitology, and histology as deemed appropriate.

All animal protocols were approved by the TAMU Animal Care and Use Committee (IACUC 2020-0003; Reference#: 142420). TAMU has NIH/PHS Approved Animal Welfare Assurance (D16-00511 (A3893-01)), and TAMU-CMP is accredited by the Association for the Assessment and Accreditation of Laboratory Animal Care (AAALAC).

Frailty Index

For all measurements, we followed established procedures (Whitehead et al., 2014). These measurements indicate age-associated deterioration of health and include the scoring of various integument, physical/musculoskeletal, ocular/nasal, digestive, and respiratory conditions. For example, integument scored alopecia, ruffled/matted coat, and piloerection. Physical/musculoskeletal conditions included tumors, distended abdomen, kyphosis, gait problems, tremors, and body weight. The ocular/nasal category covered cataracts, corneal opacity, eye discharge, and malocclusion. Diarrhea and rectal prolapse were the digestive phenotypes. Respiratory conditions observed were increased breathing rate and labored breathing. A score of 0 was assigned if no sign of frailty was observed and the animal was healthy for that phenotype. Moderate and severe phenotypes were scored as 0.5 and 1, respectively.

Whole-body composition

The analysis was conducted on live, awake animals using a quantitative nuclear magnetic resonance machine (EchoMRI-100; EchoMRI LLC; Houston, TX).

Gait measurements

Assays were performed with the DigiGait system (Mouse Specifics, Inc., Framingham, MA). Mouse paw pads were colored red with a non-toxic, washable marker and then placed on the transparent treadmill belt. The belt was started at 0° incline and 24 cm/sec speed. Video clips of 3-5 seconds were recorded once the mouse moved freely at full speed. Mice that did not move were retested once and marked as “did not move.” Mice that did not move included a few that were likely physically too frail, but mostly were mice that used the bumper to allow the belt to

drag under them without having to move. The video files were imported into the DigiGait Analysis program. After filtering out background noise, analysis graphs were generated and edited with the correct, connect, and exclude functions when necessary.

Open Field activity

Total time moving and time in the center of open field arenas were measured using the Noldus Ethovision video tracking software system (version 17.0.1630; Leesburg, VA). Arenas were sectioned into a center, inner zone, outer zone, and a thigmotaxis area along the walls. Mice acclimated to the testing room for at least 15 minutes before being placed in the center of an arena and left undisturbed. For 30 minutes, the camera system tracked their center points.

Novel Object Recognition

The assays were carried out using a layout consisting of eight gray-colored plexiglass arenas with cameras for video recording. Acquisition of video footage and analysis was done with the Noldus Ethovision software. Objects were pre-tested weeks in advance to ensure that, on average, the mice did not prefer one object over the other. The two types of objects used for the experiment were constructed of plastic Trio blocks, using slightly different blocks and placing a metal spring on one set to make the two different configurations. Objects were thought to be “climb-proof,” but specific mice still climbed on them. Time spent sitting on the objects was removed from the analysis, while quick “climb-throughs” of the objects were kept in the analysis. Eight identical sets of each of the object configurations were constructed.

The testing protocol involved the following steps. Mice in their home cages were placed in the testing room and allowed to acclimate for at least 0.5h or until their activity slowed and they rested again. Mice (8 total, one in each arena) were then placed in empty testing arenas for

a 10-minute habituation phase. Following habituation, mice were placed together back in their home cage for approximately 15 minutes. During that time, arenas were cleaned with a 2% ($^{w}/_{v}$) chlorhexidine diacetate solution (Nolvasan®), and identical objects were placed in each arena. To avoid any bias from the order of the objects (familiar vs. novel), half the arenas used one object as the familiar object; half used the other. Mice were then placed back into their same arena, now containing the identical objects, and allowed to explore for 10 minutes, called the familiarization phase. The phase was recorded to ensure that mice explored the objects for at least one minute. At the end of the familiarization, the mice were housed individually in separate holding cages for 15 minutes. During this time, arenas were cleaned with Nolvasan®, and all objects were removed and cleaned with ethanol. New object configurations were set up in each arena, one object being the familiar object seen during the previous phase and one object being the new or novel object. The novel object placement varied between the four arenas to avoid any bias in spatial preference. After 15 minutes in the holding cages, mice were placed back in the same arena for 5 minutes of recording their exploration of the familiar and novel object.

Novel object exploration was analyzed using Noldus Ethovision Analysis software. Each trial was edited to ensure correct recognition of the head vs. tail. Software arena settings were such that equal-sized regions around each object were drawn, and the software calculated the time of the mouse's nose in the area of interest around either the familiar or novel object. The amount of time the nose point was within 2cm of either object was used to calculate a discrimination index (DI) (Lueptow, 2017). The DI here was defined as the time spent exploring the novel object minus the time spent exploring the familiar object, which was then divided by total exploration time. A discrimination index greater than or equal to 0.06 was considered a preference for the novel object.

Echocardiography

Examinations were performed using the FujiFilm VisualSonics Vevo® 3100 high-frequency ultrasound system. Mice were anesthetized using an isoflurane anesthesia chamber (SomnoSuite Mouse Anesthesia System). Once unconscious, mice were placed supine on a heated imaging platform (37°C) and provided a constant flow of isoflurane for the procedure. Limbs were carefully taped over electrodes containing electrode conductivity gel to maintain body position and monitor heart rate and respiration. Nair™ hair removing lotion was used to remove fur from the thoracic region of the animal. After removing the fur and cleaning with a damp cloth, ultrasound gel was added to the animal's chest for imaging. Mouse heart rates were kept between 285 and 500 bpm for imaging. Analysis was performed with the Vevo LAB software.

Metabolic monitoring

We used PhenoMaster metabolic cages (TSE systems; Chesterfield, MO) to evaluate 32 individually housed mice (8 mice per sex per diet group). The system has small mammal gas calorimetry sensors to measure the animal's oxygen consumption and carbon dioxide production to calculate key metabolic parameters, including the respiratory exchange rate (RER). Energy expenditure, food intake, water consumption, body weight, and physical activity were simultaneously recorded over three consecutive days (72h). Only data for the last 24h of the experiment were used in the analysis to give the mice two days of acclimation to the new environment.

Blood collections

Except for the terminal collection by cardiac puncture, all other blood collections were from the submandibular (facial) vein. The professional staff of TAMU-CMP did all the collections. For the

terminal collection, each mouse was euthanized in a carbon dioxide chamber, and a cardiac puncture was performed soon after. Blood was placed in sample tubes with a clotting activator/gel and allowed to clot for at least 20 minutes. Tubes were then spun at 5,000*g* for 5 minutes. The clarified serum was aliquoted and stored at -80°C.

Complete blood counts (CBC)

Samples were in Microvette® CB 300 EDTA K2E capillary blood collection tubes. The tubes were inverted 10-15 times again before measuring with the Abaxis VetScan HM5 Color Hematology System.

Inflammatory Cytokines and Chemokines

Serum samples were sent to Eve Technologies (Calgary, Alberta, Canada) and measured with multiplex laser bead array technology (test MD32). The measurements for each mouse sample were done in duplicate.

Fecal sample collection for microbiome analysis

Mouse fecal pellets were gathered by positioning the mice on a paper towel beneath an overturned glass beaker. A minimum of three fecal pellets from each animal were transferred into cryovials using sterile forceps. The samples were preserved at -80°C and shipped to Zymo Research, where they were processed for metagenomic analyses according to their established procedures.

Serum folate assays

Liver and serum folate concentrations were measured by the *Lactobacillus casei* (*L. casei*) microbiological assay as previously described (Suh et al., 2000). *L. casei* growth was quantified at 595 nm on an Epoch Microplate Spectrophotometer (Biotek Instruments). Total folate measurements for the liver samples were normalized to protein concentration as measured using the Lowry-Bensadoun Assay (Bensadoun and Weinstein, 1976).

Uracil in genomic DNA

Liver genomic DNA was isolated using the High Pure PCR Template Preparation Kit (Roche), followed by RNAse A treatment. As previously described, two micrograms of DNA were treated with uracil DNA glycosylase (Heyden et al., 2023). Samples were derivatized, and uracil levels were quantified using gas chromatography-mass spectrometry (Fiddler et al., 2021).

Histopathology

Following euthanasia, ten organs were harvested from each mouse (see Figure 6 - Supplement 1). The samples were then fixed in 10% neutral buffered formalin at room temperature for 48h and stored in 70% ethanol until processing. Tissue sections were processed using Leica ASP300 Tissue Processor for 4h before being embedded in paraffin. The paraffin-embedded samples were sectioned at 5µm, followed by hematoxylin and eosin (H&E) staining, using a Leica HistoCore SPECTRA stainer. In a blinded manner, a board-certified veterinary pathologist (L.G.A.) evaluated histologic sections of all tissues using brightfield microscopy, scoring tissue damage on a scale from 0 to 4.

Metabolomic profiling

The untargeted, primary metabolite and biogenic amine analyses were done at the West Coast Metabolomics Center at the University of California at Davis, according to their established mass spectrometry protocols. Extract preparation was also done at the same facility from ~10mg of liver tissue in each sample, provided frozen (at -80°C). To identify significant differences in the comparisons among the different groups, we used the robust bootstrap ANOVA via the t1waybt function of the WRS2 R language package (Mair and Wilcox, 2020). Detected species that could not be assigned to any compound were excluded from the analysis.

Amino acid analysis

Serum samples were used for the PTH-based amino acid analyses (Heinrikson and Meredith, 1984) done at the Texas A&M Protein Chemistry Facility. Statistical tests for significant differences between the different strains were done as described above for the other metabolites.

DNAge analysis

Liver samples (~15mg) collected at euthanasia were placed in 0.75mL of 1X DNA/RNA Shield™ solution (Zymo Research, Irvine, CA), shipped to Zymo Research, and processed according to their established protocols.

RNA preparation from liver tissue

Liver samples were collected at euthanasia and stored at -80°C in 1X DNA/RNA Shield™ from Zymo Research. For RNA extraction, approximately 15mg of the stored liver tissue was resuspended in 0.3mL of fresh DNA/RNA Shield™ and processed using Zymo Research's Quick-RNA™ Miniprep Plus Kit. Extraction was performed according to the manufacturer's

protocol with Proteinase K digestion for 4h at room temperature, followed by a brief centrifugation to remove particulate debris. RNA lysis buffer from the kit was added to the clarified supernatant, and column purification with DNase I treatment was again performed according to the manufacturer's protocol. RNA was eluted in water and stored at -80°C.

RNAseq

Initial Quality Control was done for library construction to assess RNA concentration, OD ratios, and integrity. mRNA was isolated from 150ng total RNA using a Nextflex Poly-A Selection kit (Perkin Elmer, Waltham, MA, USA). cDNA libraries were prepared using a Nextflex Rapid Directional RNA 2.0 kit, miniaturized to 2/5 reaction volume, and automated on a Sciclone NGSx liquid handler. The 39 libraries were pooled by equal mass. The pool was sequenced on one Illumina NovaSeq S1 flowcell using the paired-end 2x50 bp recipe, which yielded 1,778 million raw clusters, with an average of 45 million clusters per sample. The sequencing raw data were mapped and quantified using the DRAGEN RNASEq pipeline with default parameters on a DRAGEN Bio-IT Platform with FPGA acceleration. 11% of the bases were trimmed based on quality (minimum quality of 24) and adapters (Stringency of 5). The resulting reads had an average mapping rate of 85% across the samples. The reference genome used was Mouse Build 39 Jun 2020, GCA_000001635.9. Transcript per million (TPM) values were used in all downstream analyses. All the data have been deposited to the Gene Expression Omnibus (GEO; Accession GSE245438) and are publicly available.

Immunoblots

In all cases we used liver tissue samples collected at euthanasia. Approximately 20mg of frozen liver tissue stored in -80°C was placed into 0.1mL cold RIPA buffer (150 mM NaCl, 1.0%

IGEPAL® CA-630, 0.5% sodium deoxycholate, 0.1% SDS, 50 mM Tris, pH 8.0) containing protease and phosphatase inhibitors. Tissues were manually homogenized with a disposable pestle and microcentrifuge tube. Sample volume was brought to 0.4mL with additional cold RIPA buffer and the lysates were centrifuged at 12,000rpm. Clarified lysate was transferred to a new tube and an aliquot removed for immunoblotting. Two gels were loaded for each set of samples, one to detect total RPS6, the other to be used for detection of phosphorylated RPS6. RPS6 phosphorylation was detected by a specific rabbit monoclonal antibody against phosphorylated Ser235/236 of the human RPS6 protein, followed by an HRP-conjugated anti-rabbit secondary antibody (see Key Resources Table). Total amounts of RPS6 were detected with a rabbit anti-RPS6 polyclonal antibody (see Key Resources Table). The phosphorylated RPS6 signal from each mouse sample was divided by the total RPS6 signal in that sample. To account for spurious differences arising among the different gels, on each gel we run samples from the same sex, but from the two diet groups. Then, each P-RPS6:RPS6 ratio was divided by the average of these ratios from all the samples on that gel (i.e., from both diet groups), and these are the values used to generate Figure 7 - Supplement 1. The raw immunoblots are in Figure 7_S1 - source data.

ELISAs

We used commercially available kits to measure serum levels of IGF-1 (see Key Resources Table) according to the manufacturer's instructions. Measurements were taken using a Tecan SPARK instrument.

Statistical Analysis

Data were analyzed using the latest version of the R language. The corresponding R packages and tests are described in the text in each case. Briefly, longitudinal measurements were

evaluated with mixed effects models using the lme4 and lmer packages. A typical function had the following syntax: lmer('measurements' ~ diet + time + sex + (1|ID), data = 'dataset'). It fits a model where 'measurements' is the response variable, and 'diet', 'time', and 'sex' are the fixed effects. 'ID' is an individual mouse, considered as a random effect to account for the non-independence of measurements within the same subject. This was a typical setup for a longitudinal evaluation where multiple measurements were taken from the same subjects over time. For survival analyses, we used the survival package. For group comparisons of non-longitudinal data, we used the non-parametric Wilcoxon rank-sum test, implemented with the base "wilcox.test" R function, or the robust bootstrap ANOVA, implemented with the "t1waybt" function of the WRS2 package. All the replicates in every experiment shown were biological ones. The number of biological replicates analyzed in each case is indicated in the text and the corresponding figures. No data or outliers were excluded from any analysis.

ACKNOWLEDGEMENTS

We acknowledge the use of several Texas A&M University core facilities, including: The Rodent Preclinical Phenotyping Core, the mouse housing facilities of the Comparative Medicine Program (CMP), the Protein Chemistry Laboratory of the Department of Biochemistry and Biophysics, and the Genomics and Bioinformatics Service. We thank Dmitry Kurouski (Texas A&M University) for making available his Tecan plate readers for ELISA-based measurements. This work was supported by a Texas A&M T3 award to M.P., H.L.A-P., and R.S.. NIH grants support M.P. (R01GM123139), L.G.A. (R01HL148153-01A1 and R21AI153879).

REFERENCES

Almeida EB, Santos JMB, Paixão V, Amaral JB, Foster R, Sperandio A, Roseira T, Rossi M, Cordeiro TG, Monteiro FR, Amirato GR, Santos CAF, Vieira RP, Vaisberg M, Barros MP, Bachi ALL. 2020. L-Glutamine Supplementation Improves the Benefits of Combined-Exercise Training on Oral Redox Balance and Inflammatory Status in Elderly Individuals. *Oxid Med Cell Longev* **2020**:2852181. doi:10.1155/2020/2852181

Annibal A, Tharyan RG, Schonewolff MF, Tam H, Latza C, Auler MMK, Grönke S, Partridge L, Antebi A. 2021. Regulation of the one carbon folate cycle as a shared metabolic signature of longevity. *Nat Commun* **12**:3486. doi:10.1038/s41467-021-23856-9

Asby DJ, Cuda F, Beyaert M, Houghton FD, Cagampang FR, Tavassoli A. 2015. AMPK Activation via Modulation of De Novo Purine Biosynthesis with an Inhibitor of ATIC Homodimerization. *Chem Biol* **22**:838–848. doi:10.1016/j.chembiol.2015.06.008

Ashburner M, Ball CA, Blake JA, Botstein D, Butler H, Cherry JM, Davis AP, Dolinski K, Dwight SS, Eppig JT, Harris MA, Hill DP, Issel-Tarver L, Kasarskis A, Lewis S, Matese JC, Richardson JE, Ringwald M, Rubin GM, Sherlock G. 2000. Gene ontology: tool for the unification of biology. The Gene Ontology Consortium. *Nat Genet* **25**:25–29. doi:10.1038/75556

Austad SN, Hoffman JM. 2018. Is antagonistic pleiotropy ubiquitous in aging biology? *Evol Med Public Health* **2018**:287–294. doi:10.1093/emph/eoy033

Barbet NC, Schneider U, Helliwell SB, Stansfield I, Tuite MF, Hall MN. 1996. TOR controls translation initiation and early G1 progression in yeast. *Mol Biol Cell* **7**:25–42.

Barcena C, Quiros PM, Durand S, Mayoral P, Rodriguez F, Caravia XM, Marino G, Garabaya C, Fernandez-Garcia MT, Kroemer G, Freije JMP, Lopez-Otin C. 2018. Methionine Restriction Extends Lifespan in Progeroid Mice and Alters Lipid and Bile Acid Metabolism. *Cell Rep* **24**:2392–2403. doi:10.1016/j.celrep.2018.07.089

Bellantuono I, de Cabo R, Ehninger D, Di Germanio C, Lawrie A, Miller J, Mitchell SJ, Navas-Enamorado I, Potter PK, Tchkonia T, Trejo JL, Lamming DW. 2020. A toolbox for the longitudinal assessment of healthspan in aging mice. *Nat Protoc* **15**:540–574. doi:10.1038/s41596-019-0256-1

Bensadoun A, Weinstein D. 1976. Assay of proteins in the presence of interfering materials. *Anal Biochem* **70**:241–250. doi:10.1016/s0003-2697(76)80064-4

Ben-Sahra I, Hoxhaj G, Ricoult SJH, Asara JM, Manning BD. 2016. mTORC1 induces purine synthesis through control of the mitochondrial tetrahydrofolate cycle. *Science* **351**:728–733. doi:10.1126/science.aad0489

Blagosklonny MV. 2010. Revisiting the antagonistic pleiotropy theory of aging: TOR-driven program and quasi-program. *Cell Cycle Georget Tex* **9**:3151–3156. doi:10.4161/cc.9.16.13120

Boelens PG, Nijveldt RJ, Houdijk AP, Meijer S, van Leeuwen PA. 2001. Glutamine alimentation in catabolic state. *J Nutr* **131**:2569S–77S; discussion 2590S. doi:10.1093/jn/131.9.2569S

Chon J, Field MS, Stover PJ. 2019. Deoxyuracil in DNA and disease: Genomic signal or managed situation? *DNA Repair* **77**:36–44. doi:10.1016/j.dnarep.2019.02.014

Chong J, Yamamoto M, Xia J. 2019. MetaboAnalystR 2.0: From Raw Spectra to Biological Insights. *Metabolites* **9**:57. doi:10.3390/metabo9030057

Cooper BA, Jonas E. 1973. Superiority of simplified assay for folate with Lactobacillus casei ATCC 7469 over assay with chloramphenicol-adapted strain. *J Clin Pathol* **26**:963–967.

Das KC, Das M, Mohanty D, Jadaon MM, Gupta A, Marouf R, Easow SK. 2005. Megaloblastosis: from morphos to molecules. *Med Princ Pract Int J Kuwait Univ Health Sci Cent* **14 Suppl 1**:2–14. doi:10.1159/000086179

Di Francesco, A., Deighan, A.G., Litichevskiy, L., Chen, Z., Luciano, A., Robinson, L., Garland, G., Donato, H., Schott, W., Wright, K.M., Raj, A., Prateek, G.V., Mullis, M., Hill, W., Zeidel, M., Peters, L., Harding, F., Botstein, D., Korstanje, R., Thaiss, C.A., Freund, A., Churchill, GA. 2023. Regulators of health and lifespan extension in genetically diverse mice on dietary restriction. *bioRxiv* 2023.11.28.568901. doi:10.1101/2023.11.28.568901

Ducker GS, Rabinowitz JD. 2017. One-Carbon Metabolism in Health and Disease. *Cell Metab* **25**:27–42. doi:10.1016/j.cmet.2016.08.009

Faure-Delanef L, Quéré I, Chassé JF, Guerassimenko O, Lesaulnier M, Bellet H, Zittoun J, Kamoun P, Cohen D. 1997. Methylenetetrahydrofolate reductase thermolabile variant and human longevity. *Am J Hum Genet* **60**:999–1001.

Ferguson FC, Thiersch JB, Philips FS. 1950. The action of 4-amino-N10-methyl-pteroylglutamic acid in mice, rats, and dogs. *J Pharmacol Exp Ther* **98**:293–299.

Fiddler JL, Xiu Y, Blum JE, Lamarre SG, Phinney WN, Stabler SP, Brosnan ME, Brosnan JT, Thalacker-Mercer AE, Field MS. 2021. Reduced Shmt2 Expression Impairs Mitochondrial Folate Accumulation and Respiration, and Leads to Uracil Accumulation in Mouse Mitochondrial DNA. *J Nutr* **151**:2882–2893. doi:10.1093/jn/nxab211

Field MS, Stover PJ. 2018. Safety of folic acid. *Ann N Y Acad Sci* **1414**:59–71. doi:10.1111/nyas.13499

Fox JT, Stover PJ. 2008. Folate-mediated one-carbon metabolism. *Vitam Horm* **79**:1–44. doi:10.1016/s0083-6729(08)00401-9

Freeman-Narrod M, Narrod SA. 1977. Chronic toxicity of methotrexate in mice. *J Natl Cancer Inst* **58**:735–741. doi:10.1093/jnci/58.3.735

Gene Ontology Consortium, Aleksander SA, Balhoff J, Carbon S, Cherry JM, Drabkin HJ, Ebert D, Feuermann M, Gaudet P, Harris NL, Hill DP, Lee R, Mi H, Moxon S, Mungall CJ, Muruganugan A, Mushayahama T, Sternberg PW, Thomas PD, Van Auken K, Ramsey J, Siegele DA, Chisholm RL, Fey P, Aspromonte MC, Nugnes MV, Quaglia F, Tosatto S, Giglio M, Nadendla S, Antonazzo G, Attrill H, Dos Santos G, Marygold S, Strelets V, Tabone CJ, Thurmond J, Zhou P, Ahmed SH, Asanitthong P, Luna Buitrago D, Erdol MN, Gage MC, Ali Kadhum M, Li KYC, Long M, Michalak A, Pesala A, Pritazahra A, Saverimuttu SCC, Su R, Thurlow KE, Lovering RC, Logie C, Oliferenko S, Blake J, Christie K, Corbani L, Dolan ME, Drabkin HJ, Hill DP, Ni L, Sitnikov D, Smith C, Cuzick A, Seager J, Cooper L, Elser J, Jaiswal P, Gupta P, Jaiswal P, Naithani S, Lera-Ramirez M, Rutherford K, Wood V, De Pons JL, Dwinell MR, Hayman GT, Kaldunski ML, Kwitek AE, Laulederkind SJF, Tutaj MA, Vedi M, Wang S-J, D'Eustachio P, Aimo L, Axelsen K, Bridge A, Hyka-Nouspikel N, Morgat A, Aleksander SA, Cherry JM, Engel SR, Karra K, Miyasato SR, Nash RS, Skrzypek MS, Weng S, Wong ED, Bakker E, Berardini TZ, Reiser L, Auchincloss A, Axelsen K, Argoud-Puy G, Blatter M-C, Boutet E, Breuza L, Bridge A, Casals-Casas C, Coudert E, Estreicher A, Livia Famiglietti M, Feuermann M, Gos A, Gruaz-Gumowski N, Hulo C, Hyka-Nouspikel N, Jungo F, Le Mercier P, Lieberherr D, Masson P, Morgat A, Pedruzzi I, Pourcel L, Poux S, Rivoire C, Sundaram S, Bateman A, Bowler-Barnett E, Bye-A-Jee H, Denny P, Ignatchenko A, Ishtiaq R, Lock A, Lussi Y, Magrane M, Martin MJ, Orchard S, Raposo P, Speretta E, Tyagi N, Warner K, Zaru R, Diehl AD, Lee R, Chan J, Diamantakis S, Raciti D, Zarowiecki M, Fisher M, James-Zorn C, Ponferrada V, Zorn A, Ramachandran S, Ruzicka L, Westerfield M. 2023. The Gene Ontology knowledgebase in 2023. *Genetics* **224**:iyad031. doi:10.1093/genetics/iyad031

Hansen M, Taubert S, Crawford D, Libina N, Lee SJ, Kenyon C. 2007. Lifespan extension by conditions that inhibit translation in Caenorhabditis elegans. *Aging Cell* **6**:95–110. doi:10.1111/j.1474-9726.2006.00267.x

He C, Tsuchiyama SK, Nguyen QT, Plyusnina EN, Terrill SR, Sahibzada S, Patel B, Faulkner AR, Shaposhnikov MV, Tian R, Tsuchiya M, Kaeberlein M, Moskalev AA, Kennedy BK,

Polymenis M. 2014. Enhanced longevity by ibuprofen, conserved in multiple species, occurs in yeast through inhibition of tryptophan import. *PLoS Genet* **10**:e1004860. doi:10.1371/journal.pgen.1004860

Heinrikson RL, Meredith SC. 1984. Amino acid analysis by reverse-phase high-performance liquid chromatography: precolumn derivatization with phenylisothiocyanate. *Anal Biochem* **136**:65–74.

Heyden KE, Fiddler JL, Xiu Y, Malysheva OV, Handzlik MK, Phinney WN, Stiles L, Stabler SP, Metallo CM, Caudill MA, Field MS. 2023. Reduced methionine synthase expression results in uracil accumulation in mitochondrial DNA and impaired oxidative capacity. *PNAS Nexus* **2**:pgad105. doi:10.1093/pnasnexus/pgad105

Holzenberger M, Dupont J, Ducos B, Leneuve P, Géloën A, Even PC, Cervera P, Le Bouc Y. 2003. IGF-1 receptor regulates lifespan and resistance to oxidative stress in mice. *Nature* **421**:182–187. doi:10.1038/nature01298

Johnson JE, Johnson FB. 2014. Methionine restriction activates the retrograde response and confers both stress tolerance and lifespan extension to yeast, mouse and human cells. *PLoS One* **9**:e97729. doi:10.1371/journal.pone.0097729

Johnson SC, Rabinovitch PS, Kaeberlein M. 2013. mTOR is a key modulator of ageing and age-related disease. *Nature* **493**:338–45. doi:10.1038/nature11861

Kaeberlein M, Kennedy BK. 2011. Hot topics in aging research: protein translation and TOR signaling, 2010. *Aging Cell* **10**:185–90. doi:10.1111/j.1474-9726.2010.00665.x

Kaeberlein M, Powers RW 3rd, Steffen KK, Westman EA, Hu D, Dang N, Kerr EO, Kirkland KT, Fields S, Kennedy BK. 2005. Regulation of yeast replicative life span by TOR and Sch9 in response to nutrients. *Science* **310**:1193–6. doi:10.1126/science.1115535

Kane AE, Hilmer SN, Boyer D, Gavin K, Nines D, Howlett SE, de Cabo R, Mitchell SJ. 2016. Impact of Longevity Interventions on a Validated Mouse Clinical Frailty Index. *J Gerontol A Biol Sci Med Sci* **71**:333–339. doi:10.1093/gerona/glu315

Kenyon C. 2011. The first long-lived mutants: discovery of the insulin/IGF-1 pathway for ageing. *Philos Trans R Soc Lond B Biol Sci* **366**:9–16. doi:10.1098/rstb.2010.0276

Knight R, Vrbanac A, Taylor BC, Aksenov A, Callewaert C, Debelius J, Gonzalez A, Kosciolek T, McCall L-I, McDonald D, Melnik AV, Morton JT, Navas J, Quinn RA, Sanders JG, Swafford AD, Thompson LR, Tripathi A, Xu ZZ, Zaneveld JR, Zhu Q, Caporaso JG, Dorrestein PC. 2018. Best practices for analysing microbiomes. *Nat Rev Microbiol* **16**:410–422. doi:10.1038/s41579-018-0029-9

Kozieł R, Ruckenstuhl C, Albertini E, Neuhaus M, Netzberger C, Bust M, Madeo F, Wiesner RJ, Jansen-Dürr P. 2014. Methionine restriction slows down senescence in human diploid fibroblasts. *Aging Cell* **13**:1038–1048. doi:10.1111/acel.12266

Labuschagne CF, van den Broek NJF, Mackay GM, Vousden KH, Maddocks ODK. 2014. Serine, but not glycine, supports one-carbon metabolism and proliferation of cancer cells. *Cell Rep* **7**:1248–1258. doi:10.1016/j.celrep.2014.04.045

Lee BC, Kaya A, Gladyshev VN. 2016. Methionine restriction and life-span control. *Ann N Acad Sci* **1363**:116–24. doi:10.1111/nyas.12973

Lee BC, Kaya A, Ma S, Kim G, Gerashchenko MV, Yim SH, Hu Z, Harshman LG, Gladyshev VN. 2014. Methionine restriction extends lifespan of Drosophila melanogaster under conditions of low amino-acid status. *Nat Commun* **5**:3592. doi:10.1038/ncomms4592

Lindsey ML, Kassiri Z, Virag JAI, de Castro Brás LE, Scherrer-Crosbie M. 2018. Guidelines for measuring cardiac physiology in mice. *Am J Physiol Heart Circ Physiol* **314**:H733–H752. doi:10.1152/ajpheart.00339.2017

Locasale JW. 2013. Serine, glycine and one-carbon units: cancer metabolism in full circle. *Nat Rev Cancer* **13**:572–83. doi:10.1038/nrc3557

Lopez-Otin C, Blasco MA, Partridge L, Serrano M, Kroemer G. 2013. The hallmarks of aging. *Cell* **153**:1194–217. doi:10.1016/j.cell.2013.05.039

Lueptow LM. 2017. Novel Object Recognition Test for the Investigation of Learning and Memory in Mice. *J Vis Exp JoVE* 55718. doi:10.3791/55718

Maitra N, He C, Blank HM, Tsuchiya M, Schilling B, Kaeberlein M, Aramayo R, Kennedy BK, Polymenis M. 2020. Translational control of one-carbon metabolism underpins ribosomal protein phenotypes in cell division and longevity. *eLife* **9**:e53127. doi:10.7554/eLife.53127

Mason JB, Dickstein A, Jacques PF, Haggarty P, Selhub J, Dallal G, Rosenberg IH. 2007. A temporal association between folic acid fortification and an increase in colorectal cancer rates may be illuminating important biological principles: a hypothesis. *Cancer Epidemiol Biomark Prev Publ Am Assoc Cancer Res Cosponsored Am Soc Prev Oncol* **16**:1325–1329. doi:10.1158/1055-9965.EPI-07-0329

McCormick MA, Delaney JR, Tsuchiya M, Tsuchiyama S, Shemorry A, Sim S, Chou AC, Ahmed U, Carr D, Murakami CJ, Schleit J, Sutphin GL, Wasko BM, Bennett CF, Wang AM, Olsen B, Beyer RP, Bammler TK, Prunkard D, Johnson SC, Pennypacker JK, An E, Anies A, Castanza AS, Choi E, Dang N, Enerio S, Fletcher M, Fox L, Goswami S, Higgins SA, Holmberg MA, Hu D, Hui J, Jelic M, Jeong KS, Johnston E, Kerr EO, Kim J, Kim D, Kirkland K, Klum S, Kotireddy S, Liao E, Lim M, Lin MS, Lo WC, Lockshon D, Miller HA, Moller RM, Muller B, Oakes J, Pak DN, Peng ZJ, Pham KM, Pollard TG, Pradeep P, Pruett D, Rai D, Robison B, Rodriguez AA, Ros B, Sage M, Singh MK, Smith ED, Snead K, Solanky A, Spector BL, Steffen KK, Tchao BN, Ting MK, Vander Wende H, Wang D, Welton KL, Westman EA, Brem RB, Liu XG, Suh Y, Zhou Z, Kaeberlein M, Kennedy BK. 2015. A Comprehensive Analysis of Replicative Lifespan in 4,698 Single-Gene Deletion Strains Uncovers Conserved Mechanisms of Aging. *Cell Metab* **22**:895–906. doi:10.1016/j.cmet.2015.09.008

Meyuhas O. 2015. Ribosomal Protein S6 Phosphorylation: Four Decades of Research. *Int Rev Cell Mol Biol* **320**:41–73. doi:10.1016/bs.ircmb.2015.07.006

Miller RA, Buehner G, Chang Y, Harper JM, Sigler R, Smith-Wheelock M. 2005. Methionine-deficient diet extends mouse lifespan, slows immune and lens aging, alters glucose, T4, IGF-I and insulin levels, and increases hepatocyte MIF levels and stress resistance. *Aging Cell* **4**:119–125. doi:10.1111/j.1474-9726.2005.00152.x

Montoliu I, Scherer M, Beguelin F, DaSilva L, Mari D, Salvioli S, Martin F-PJ, Capri M, Bucci L, Ostan R, Garagnani P, Monti D, Biagi E, Brigidi P, Kussmann M, Rezzi S, Franceschi C, Collino S. 2014. Serum profiling of healthy aging identifies phospho- and sphingolipid species as markers of human longevity. *Aging* **6**:9–25.

Orentreich N, Matias JR, DeFelice A, Zimmerman JA. 1993. Low methionine ingestion by rats extends life span. *J Nutr* **123**:269–274. doi:10.1093/jn/123.2.269

Philips FS, Thiersch JB, Ferguson FC. 1950. Studies of the action of 4-aminopteroylglutamic acid and its congeners in mammals. *Ann N Y Acad Sci* **52**:1349–1359. doi:10.1111/j.1749-6632.1950.tb54036.x

Promislow DEL. 2004. Protein networks, pleiotropy and the evolution of senescence. *Proc Biol Sci* **271**:1225–1234. doi:10.1098/rspb.2004.2732

Qiu A, Jansen M, Sakaris A, Min SH, Chattopadhyay S, Tsai E, Sandoval C, Zhao R, Akabas MH, Goldman ID. 2006. Identification of an intestinal folate transporter and the molecular basis for hereditary folate malabsorption. *Cell* **127**:917–928. doi:10.1016/j.cell.2006.09.041

Rajagopalan PTR, Zhang Z, McCourt L, Dwyer M, Benkovic SJ, Hammes GG. 2002. Interaction of dihydrofolate reductase with methotrexate: Ensemble and single-molecule kinetics. *Proc Natl Acad Sci U S A* **99**:13481–13486. doi:10.1073/pnas.172501499

Reeves PG, Nielsen FH, Fahey GC. 1993. AIN-93 purified diets for laboratory rodents: final report of the American Institute of Nutrition ad hoc writing committee on the reformulation of the AIN-76A rodent diet. *J Nutr* **123**:1939–1951. doi:10.1093/jn/123.11.1939

Reina-Campos M, Diaz-Meco MT, Moscat J. 2019. The complexity of the serine glycine one-carbon pathway in cancer. *J Cell Biol*. doi:10.1083/jcb.201907022

Rosenzweig A, Blenis J, Gomes AP. 2018. Beyond the Warburg Effect: How Do Cancer Cells Regulate One-Carbon Metabolism? *Front Cell Dev Biol* **6**:90. doi:10.3389/fcell.2018.00090

Ruckenstuhl C, Netzberger C, Entfellner I, Carmona-Gutierrez D, Kickenweiz T, Stekovic S, Gleixner C, Schmid C, Klug L, Sorgo AG, Eisenberg T, Buttner S, Marino G, Koziel R, Jansen-Durr P, Frohlich KU, Kroemer G, Madeo F. 2014. Lifespan extension by methionine restriction requires autophagy-dependent vacuolar acidification. *PLoS Genet* **10**:e1004347. doi:10.1371/journal.pgen.1004347

Rustia M, Shubik P. 1973. Life-span carcinogenicity tests with 4-amino-N10-methylpteroylglutamic acid (methotrexate) in Swiss mice and Syrian golden hamsters. *Toxicol Appl Pharmacol* **26**:329–338. doi:10.1016/0041-008x(73)90269-x

Salojin KV, Cabrera RM, Sun W, Chang WC, Lin C, Duncan L, Platt KA, Read R, Vogel P, Liu Q, Finnell RH, Oravecz T. 2011. A mouse model of hereditary folate malabsorption: deletion of the PCFT gene leads to systemic folate deficiency. *Blood* **117**:4895–4904. doi:10.1182/blood-2010-04-279653

Scholl TO, Johnson WG. 2000. Folic acid: influence on the outcome of pregnancy. *Am J Clin Nutr* **71**:1295S–303S. doi:10.1093/ajcn/71.5.1295s

Scott JM, Weir DG. 1980. Drug-induced megaloblastic change. *Clin Haematol* **9**:587–606.

Segata N, Izard J, Waldron L, Gevers D, Miropolsky L, Garrett WS, Huttenhower C. 2011. Metagenomic biomarker discovery and explanation. *Genome Biol* **12**:R60. doi:10.1186/gb-2011-12-6-r60

Soma S, Yang K, Morales MI, Polymenis M. 2014. Multiple metabolic requirements for size homeostasis and initiation of division in Saccharomyces cerevisiae. *Microb Cell* **1**:256–266. doi:10.15698/mic2014.08.160

Soysal P, Smith L, Capar E, Kalan U, Arik F, Isik AT. 2019. Vitamin B12 and folate deficiencies are not associated with nutritional or weight status in older adults. *Exp Gerontol* **116**:1–6. doi:10.1016/j.exger.2018.12.007

Steffen KK, Kennedy BK, Kaeberlein M. 2009. Measuring Replicative Life Span in the Budding Yeast. *J Vis Exp* e1209. doi:10.3791/1209

Steffen KK, MacKay VL, Kerr EO, Tsuchiya M, Hu D, Fox LA, Dang N, Johnston ED, Oakes JA, Tchao BN. 2008. Yeast life span extension by depletion of 60s ribosomal subunits is mediated by Gcn4. *Cell* **133**:292–302. doi:10.1016/j.cell.2008.02.037

Steffen KK, McCormick MA, Pham KM, MacKay VL, Delaney JR, Murakami CJ, Kaeberlein M, Kennedy BK. 2012. Ribosome deficiency protects against ER stress in Saccharomyces cerevisiae. *Genetics* **191**:107–18. doi:10.1534/genetics.111.136549

Suh JR, Oppenheim EW, Girgis S, Stover PJ. 2000. Purification and properties of a folate-catabolizing enzyme. *J Biol Chem* **275**:35646–35655. doi:10.1074/jbc.M005864200

Sun L, Sadighi Akha AA, Miller RA, Harper JM. 2009. Life-span extension in mice by preweaning food restriction and by methionine restriction in middle age. *J Gerontol A Biol Sci Med Sci* **64**:711–722. doi:10.1093/gerona/glp051

Sutphin GL, Kaeberlein M. 2009. Measuring Caenorhabditis elegans Life Span on Solid Media. *J Vis Exp* e1152. doi:10.3791/1152

Suzuki T, Chéret J, Scala FD, Akhundlu A, Gherardini J, Demetrius D-L, O'Sullivan JDB, Kuka Epstein G, Bauman AJ, Demetriades C, Paus R. 2023. mTORC1 activity negatively regulates human hair follicle growth and pigmentation. *EMBO Rep* **24**:e56574. doi:10.15252/embr.202256574

Thomas PD, Ebert D, Muruganujan A, Mushayahama T, Albou L-P, Mi H. 2022. PANTHER:

Making genome-scale phylogenetics accessible to all. *Protein Sci Publ Protein Soc* **31**:8–22. doi:10.1002/pro.4218

Turturro A, Witt WW, Lewis S, Hass BS, Lipman RD, Hart RW. 1999. Growth curves and survival characteristics of the animals used in the Biomarkers of Aging Program. *J Gerontol A Biol Sci Med Sci* **54**:B492-501. doi:10.1093/gerona/54.11.b492

Virk B, Jia J, Maynard CA, Raimundo A, Lefebvre J, Richards SA, Chetina N, Liang Y, Helliwell N, Cipinska M, Weinkove D. 2016. Folate Acts in E. coli to Accelerate C. elegans Aging Independently of Bacterial Biosynthesis. *Cell Rep* **14**:1611–1620. doi:10.1016/j.celrep.2016.01.051

Visentin M, Diop-Bove N, Zhao R, Goldman ID. 2014. The intestinal absorption of folates. *Annu Rev Physiol* **76**:251–274. doi:10.1146/annurev-physiol-020911-153251

West MG, Horne DW, Appling DR. 1996. Metabolic role of cytoplasmic isozymes of 5,10-methylenetetrahydrofolate dehydrogenase in Saccharomyces cerevisiae. *Biochemistry* **35**:3122–3132. doi:10.1021/bi952713d

Whitehead JC, Hildebrand BA, Sun M, Rockwood MR, Rose RA, Rockwood K, Howlett SE. 2014. A clinical frailty index in aging mice: comparisons with frailty index data in humans. *J Gerontol A Biol Sci Med Sci* **69**:621–632. doi:10.1093/gerona/glt136

Williams GC. 1957. Pleiotropy, Natural-Selection, and the Evolution of Senescence. *Evolution* **11**:398–411. doi:10.2307/2406060

Wu X, Xie Wei, Xie Wenxuan, Wei W, Guo J. 2022. Beyond controlling cell size: functional analyses of S6K in tumorigenesis. *Cell Death Dis* **13**:646. doi:10.1038/s41419-022-05081-4

Yuan R, Tsaih S-W, Petkova SB, Marin de Evsikova C, Xing S, Marion MA, Bogue MA, Mills KD, Peters LL, Bult CJ, Rosen CJ, Sundberg JP, Harrison DE, Churchill GA, Paigen B. 2009. Aging in inbred strains of mice: study design and interim report on median lifespans and circulating IGF1 levels. *Aging Cell* **8**:277–287. doi:10.1111/j.1474-9726.2009.00478.x

Zhang WB, Ye K, Barzilai N, Milman S. 2021. The antagonistic pleiotropy of insulin-like growth factor 1. *Aging Cell* **20**:e13443. doi:10.1111/acel.13443

Zheng Y, Cantley LC. 2019. Toward a better understanding of folate metabolism in health and disease. *J Exp Med* **216**:253–266. doi:10.1084/jem.20181965

Zou K, Rouskin S, Dervishi K, McCormick MA, Sasikumar A, Deng C, Chen Z, Kaeberlein M, Brem RB, Polymenis M, Kennedy BK, Weissman JS, Zheng J, Ouyang Q, Li H. 2020. Life span extension by glucose restriction is abrogated by methionine supplementation: Cross-talk between glucose and methionine and implication of methionine as a key regulator of life span. *Sci Adv* **6**:eaba1306. doi:10.1126/sciadv.aba1306

FIGURES AND FIGURE LEGENDS

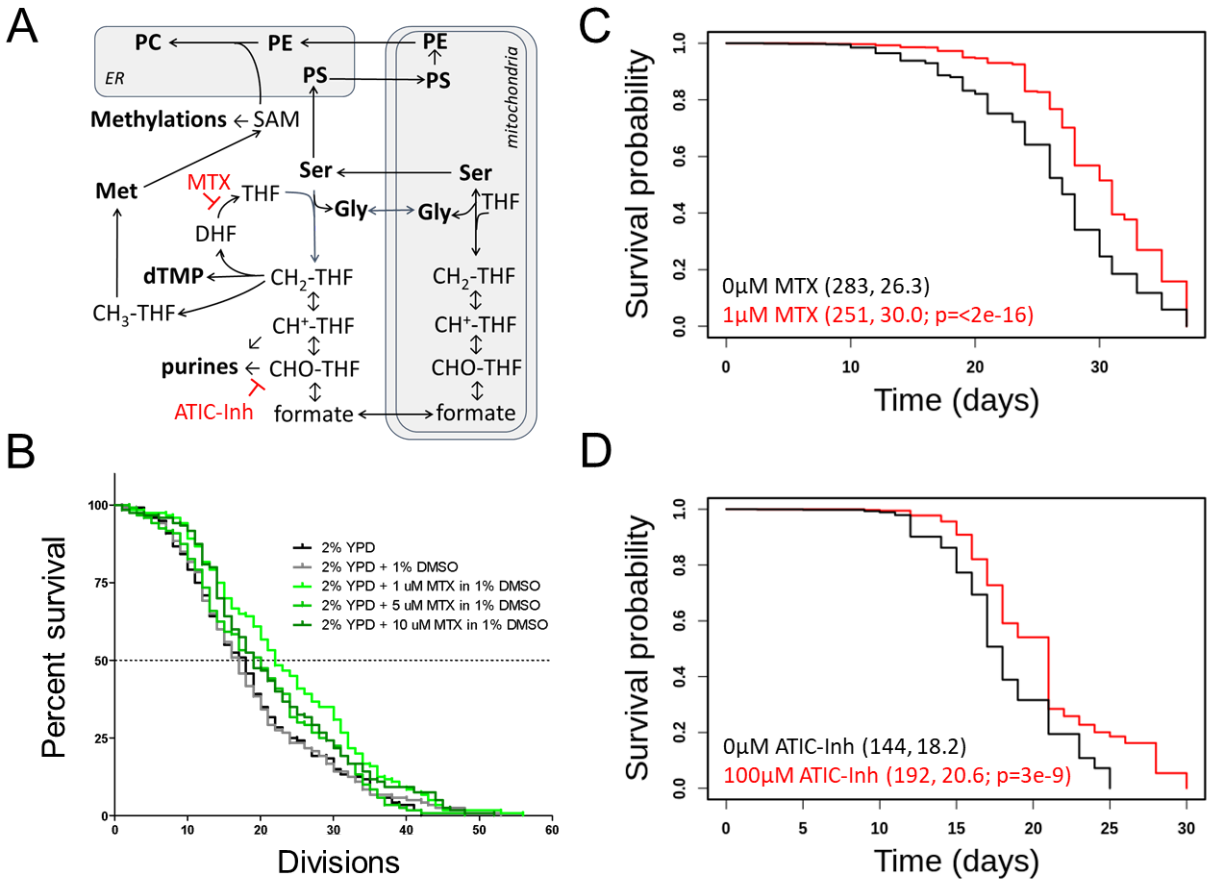

FIGURE 1. Inhibitors of 1C metabolism extend the lifespan of yeast and worms. (**A**) Schematic of 1C enzymatic reactions. The reactions inhibited by methotrexate (MTX) or ATIC Dimerization Inhibitor (ATIC-Inh) are indicated. (**B**) Survival curves on rich undefined media (YPD) for *S. cerevisiae* MATα (strain BY4742) cells (shown in black), compared to experiment-matched cells mock-treated with DMSO (shown in gray) or three different doses of MTX (as indicated, in different shades of green). The number of mother cell divisions (replicative lifespan) is on the x-axis. (**C**) Survival curves for *C. elegans* (strain N2) exposed to the indicated doses of MTX. Survival probability is on the y-axis, and time (in days) is on the x-axis. Mean lifespans and the number of animals assayed in each case are shown in parentheses. The indicated p value was based on the log-rank test. (**D**) Survival curves, as in (C), for animals exposed to the indicated doses of ATIC-Inh.

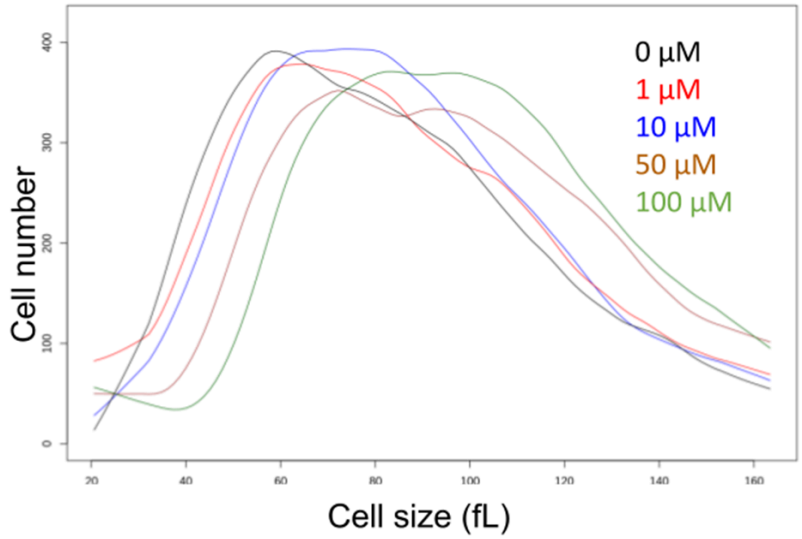

FIGURE 1 - Supplement 1. Methotrexate increases the size of yeast cells. Cell size histograms of yeast cells (BY4742 strain background) treated with the indicated doses of methotrexate. Size (in fL) is on the x-axis, and the cell number on the y-axis.

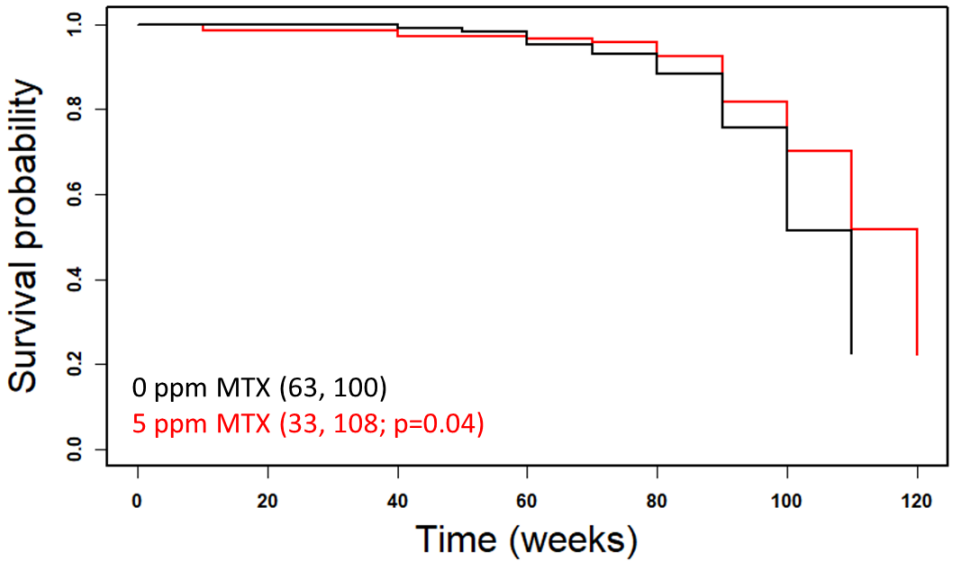

FIGURE 1 - Supplement 2. Survival curves of female Swiss mice on chronic, low-dose methotrexate (MTX). MTX was administered in the food at the indicated dose every other week, starting at 7 weeks of age. Raw data were from (Rustia and Shubik, 1973). Survival probability is on the y-axis, and time (in weeks) is on the x-axis. Mean lifespans and the number of animals assayed in each case are shown in parentheses. The indicated p value was based on the log-rank test.

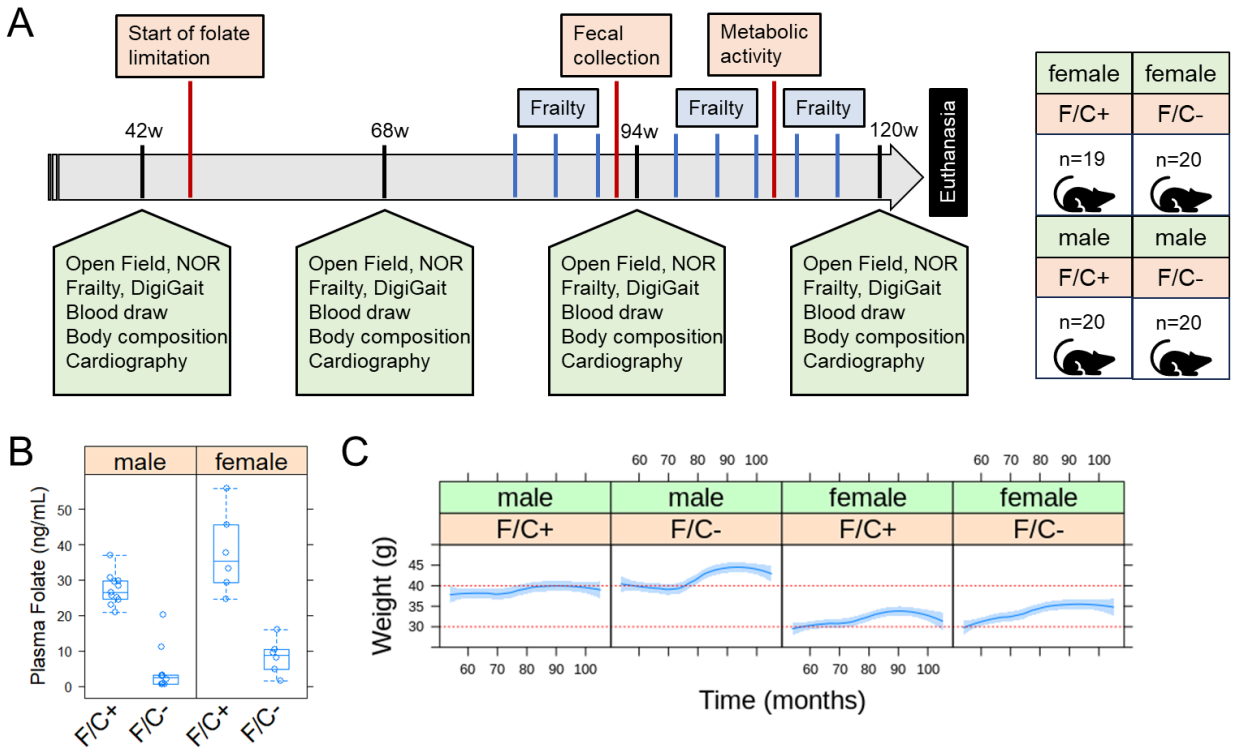

FIGURE 2. Evaluating healthspan in mice under dietary folate restriction late in life. (**A**) Schematic of the study design. See Materials and Methods for a detailed description of each assay. (**B**) Serum folate levels were measured at 120w, using an established microbiological assay (Cooper and Jonas, 1973) and shown on the y-axis. The different diets are on the x-axis, as indicated for the folate/choline-replete (F/C+) or -limited (F/C-) groups. The boxplot graphs were generated with R language functions. Each box is drawn from the first to the third quartile, with a horizontal line denoting the median. The whiskers show the interquartile range (IQR), and they were drawn at 1.5xIQR. The replicates were all biological ones from different animals. (**C**) The weight of the animals (y-axis) was measured every month (x-axis). The red horizontal lines were drawn to help visualize the weight changes over time in female and male mice. Loess curves and the std errors at a 0.95 level are shown. A mixed effects regression model was applied with the *lme4 and lmer* R language packages to evaluate the effects of the fixed variables (diet, time, sex) on the observed weight, taking into account the repeated longitudinal measurements on each mouse (see Materials and Methods, and description in the text). A negative association with the F/C+ diet was significant (p=0.0313).

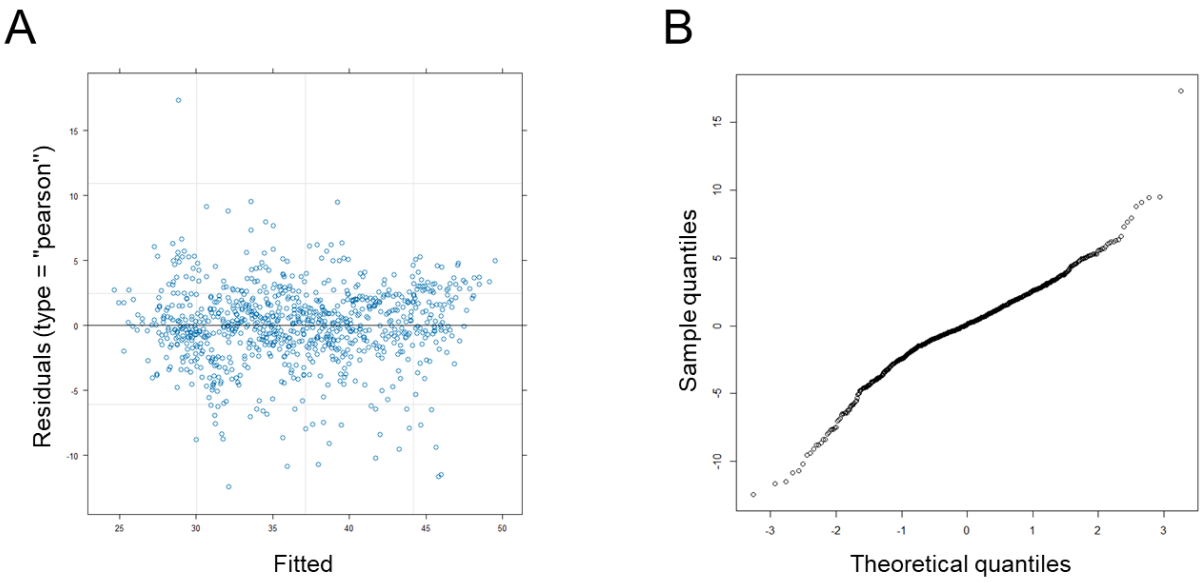

FIGURE 2 - Supplement 1. Evaluating assumptions of a linear regression model for longitudinal weight measurements. (**A**) Plot of the standardized residuals on the y-axis and the fitted values on the x-axis, from the data shown in Figure 2C. (**B**) Q-Q plot of the residuals, with the sample quantiles from the measurements in Figure 2C (y-axis), against the theoretical normally distributed ones (x-axis).

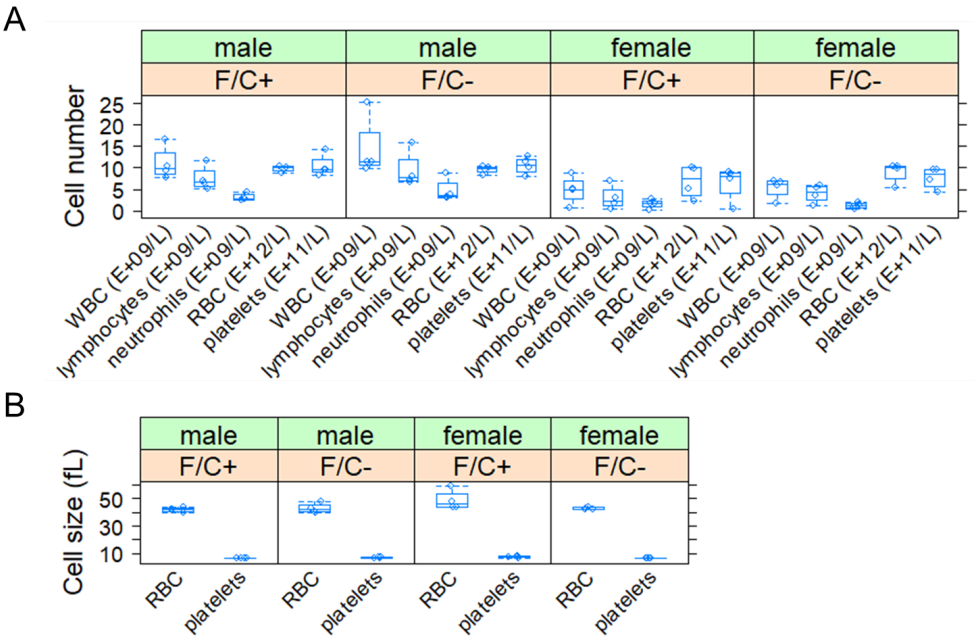

FIGURE 2 - Supplement 2. Number and size of blood cells from mice placed on dietary folate restriction late in life. (**A**) Blood cell numbers were measured at 108 weeks of age from animals of the indicated sex and diet group. (**B**) Cell size (y-axis; in fL) was measured from the same samples shown in (A) from animals of the indicated sex and diet group. The boxplots were drawn as in Figure 2.

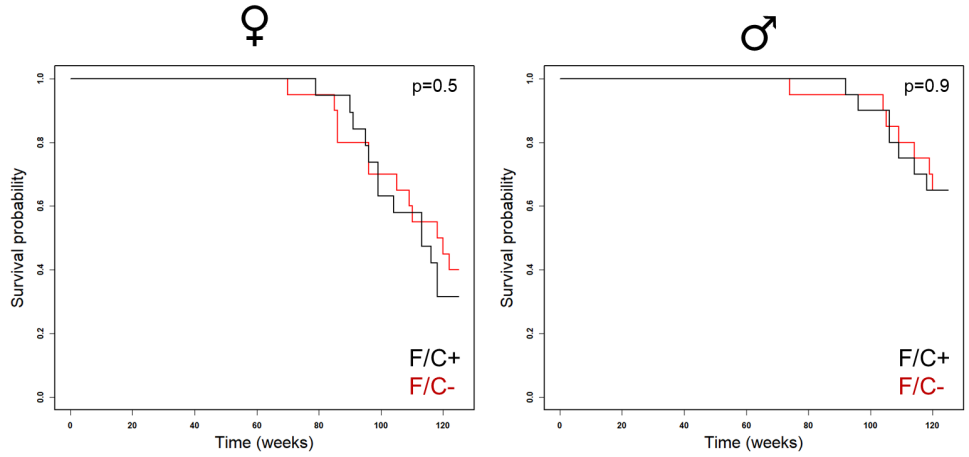

FIGURE 2 - Supplement 3. Survival curves of mice placed on dietary folate restriction late in life. Survival probability is on the y-axis, and time (in weeks) on the x-axis, from female (right panel) and male (left panel) animals of each diet test group. The indicated p value was based on the log-rank test.

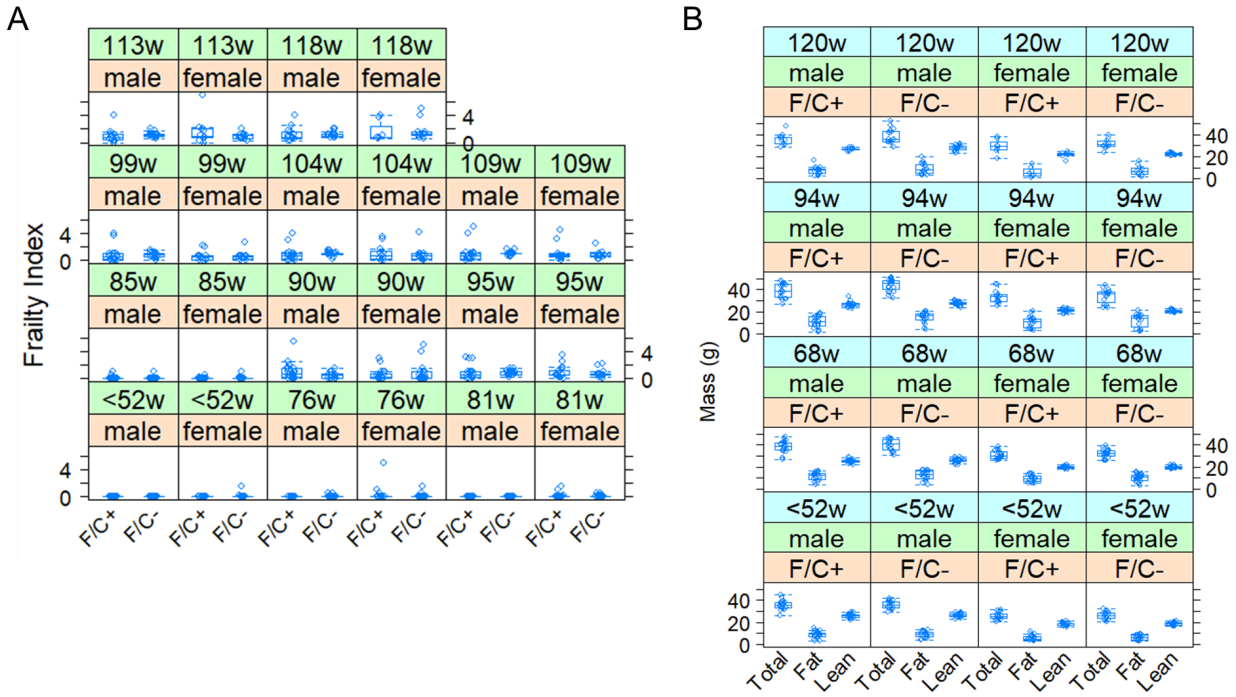

FIGURE 3. No adverse healthspan metrics in mice placed on dietary folate restriction late in life. (**A**) Frailty Index scores are shown on the y-axis. Measurements were taken at the indicated times from female and male animals of each diet test group, as described in Materials and Methods. (**B**) The total, fat, and lean mass of each mouse in the study was measured by MRI (see Materials and Methods), and shown on the y-axis. The boxplots were drawn as in Figure 2.

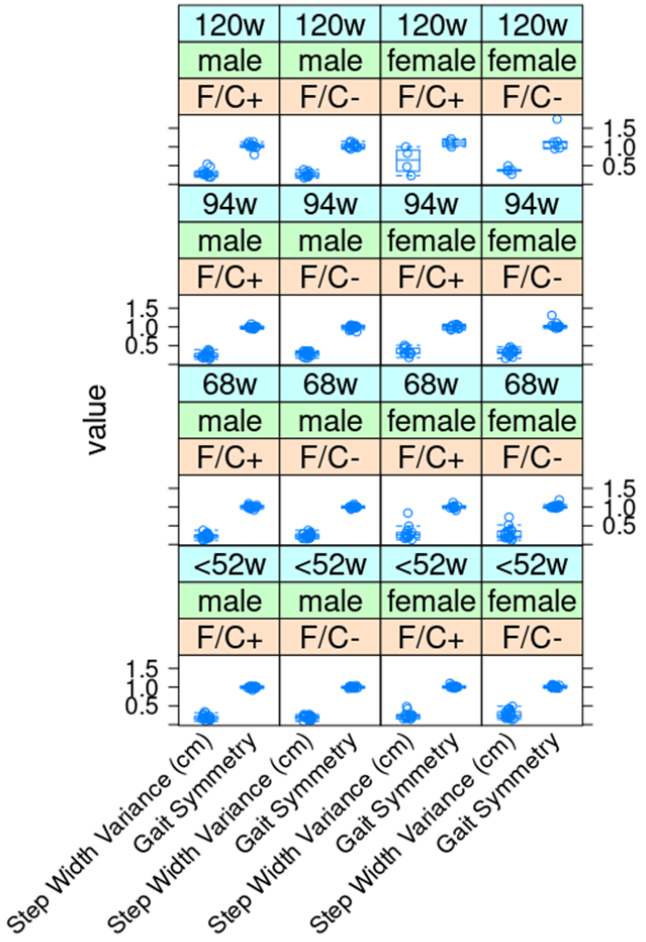

FIGURE 3 - Supplement 1. No significant gait changes in mice placed on dietary folate restriction late in life. As described in Materials and Methods, step width variance and gait symmetry values (shown on the y-axis) were measured with the Digigait system. As indicated, measurements were taken at the indicated times from female and male animals of each diet test group. The boxplots were drawn as in the previous figures.

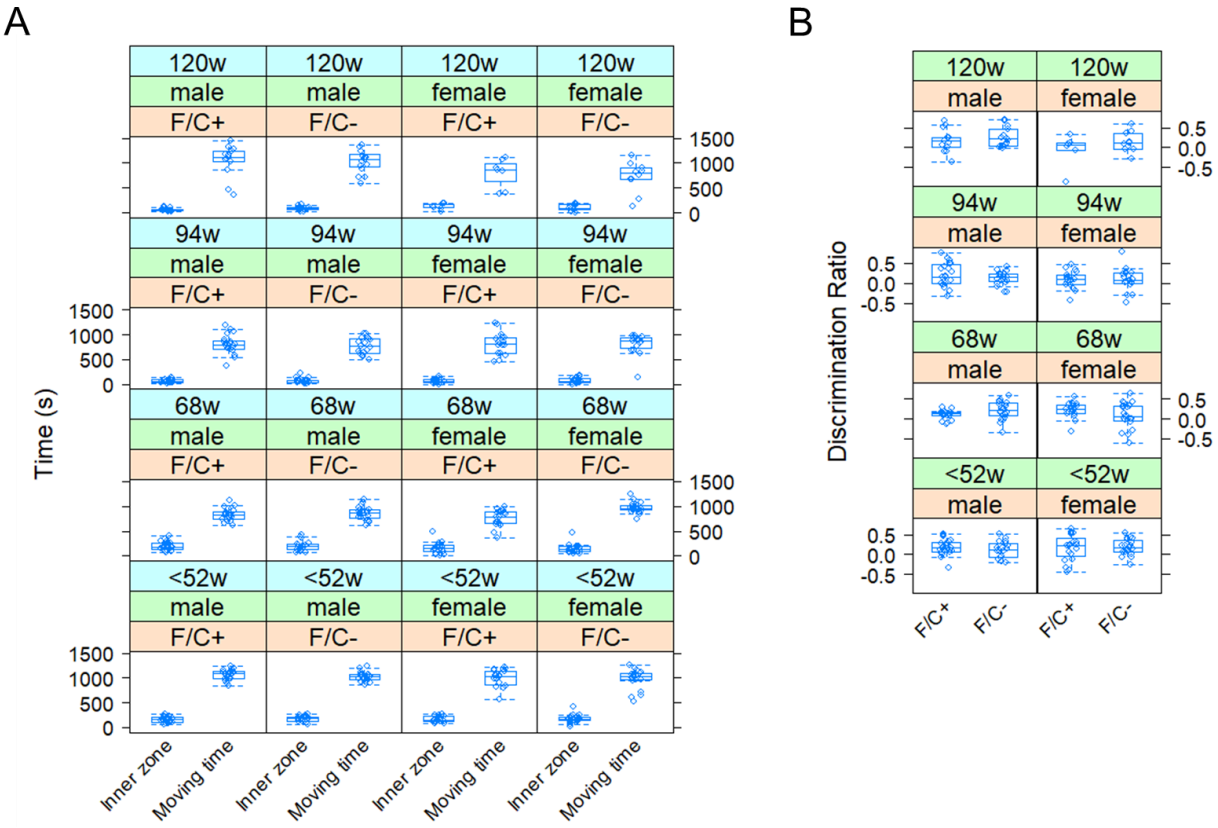

FIGURE 3 - Supplement 2. Open field (A) and novel object recognition (B) assays in mice placed on dietary folate restriction late in life. In (**A**), the inner zone and moving times during open field evaluation are on the y-axis. In (**B**), the discrimination ratio values, reflecting the ability of the mice to recognize a new object, are on the y-axis. Detailed descriptions of the assays are in Materials and Methods. The boxplots were drawn as in the previous figures.

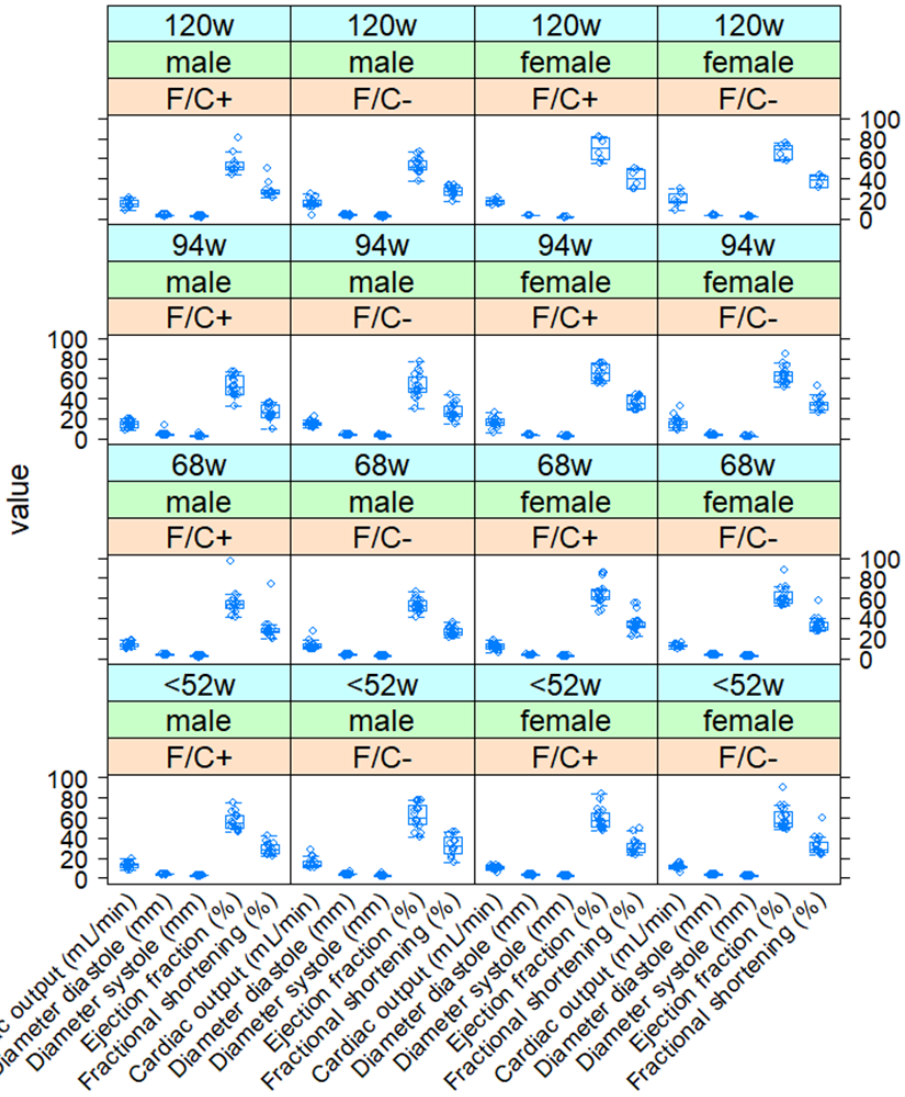

FIGURE 3 - Supplement 3. Normal cardiac function of mice placed on dietary folate restriction late in life. Several parameters of cardiac function (x-axis) were measured by echocardiography as described in Materials and Methods, and the corresponding values are on the y-axis. Measurements were taken at the indicated times from female and male animals of each diet test group, as indicated. The boxplots were drawn as in the previous figures.

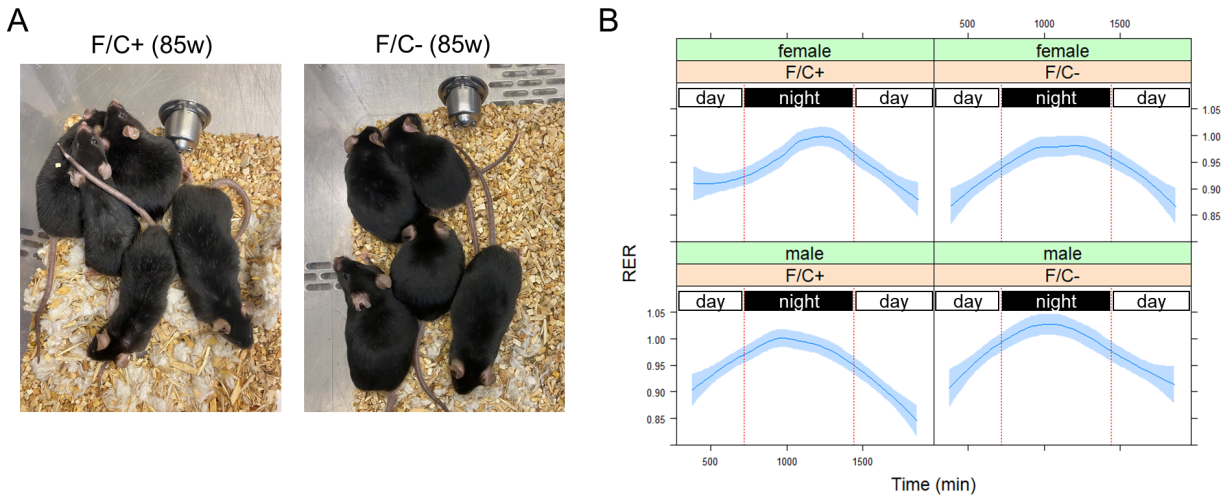

FIGURE 4. Improved metabolic activity of mice placed on dietary folate restriction late in life. (**A**) Photographs of male mice on the indicated diet were taken at 85 weeks of age. Signs of graying were visible on the coat of mice on the F/C+ diet (left) but not on the coat of mice on the F/C- diet (right). (**B**) The respiratory exchange rate (RER) values (y-axis) were from 6-8 mice in each indicated group at 108 weeks of age. The measurements were taken after the animals were acclimated for two days in the metabolic cages. The period between the red vertical lines corresponds to night-time when mice are active. Loess curves and the std errors at a 0.95 level are shown.

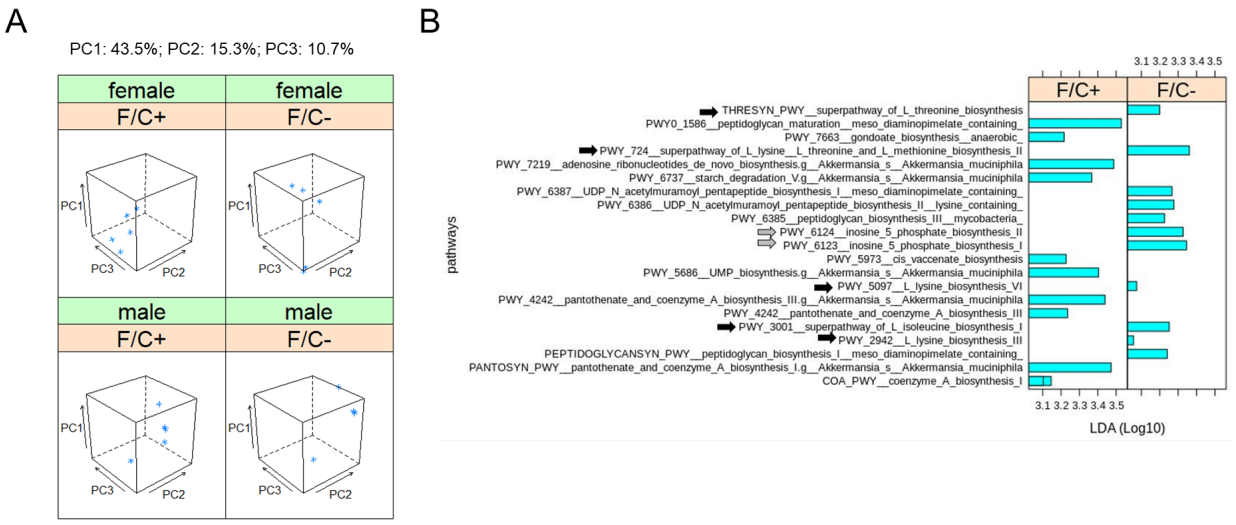

FIGURE 5. Metagenomic profiling of the gut microbiome of mice placed on dietary folate restriction late in life. (**A**) Beta diversity principal component analysis plots were based on Bray-Curtis dissimilarity indices (Knight et al., 2018), of the DNA from the fecal microbiome sampled and sequenced at 90 weeks of age, from 5 mice in each test group. Three principal components (PC1,2,3; shown at the top) accounted for ~70% of the dataset variance. (**B**) Metabolic pathway biomarker changes associated with folate limitation late in life, from metagenomic data of the fecal microbiome. The LEfSe computational pipeline was used to determine the features most likely to explain the observed differences. The computed linear discriminant analysis (LDA) scores (Log10-transformed) are on the x-axis. LDA scores incorporate effect sizes, ranking the relevance of the identified biomarkers and enabling their visualization (Segata et al., 2011). Gray arrows indicate pathways involved in amino acid synthesis and black arrows indicate pathways involved in IMP synthesis.

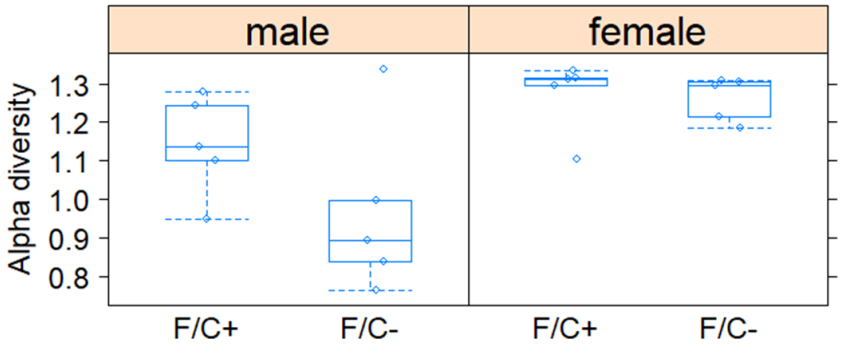

FIGURE 5 - Supplement 1. Species diversity within the gut microbiome of mice placed on dietary folate restriction late in life. Shannon's diversity index (y-axis) is shown for each sex and diet as a metric of the alpha diversity of the fecal microbiome sampled and sequenced at 90 weeks of age, from 5 mice in each test group. The boxplots were drawn as in the previous figures.

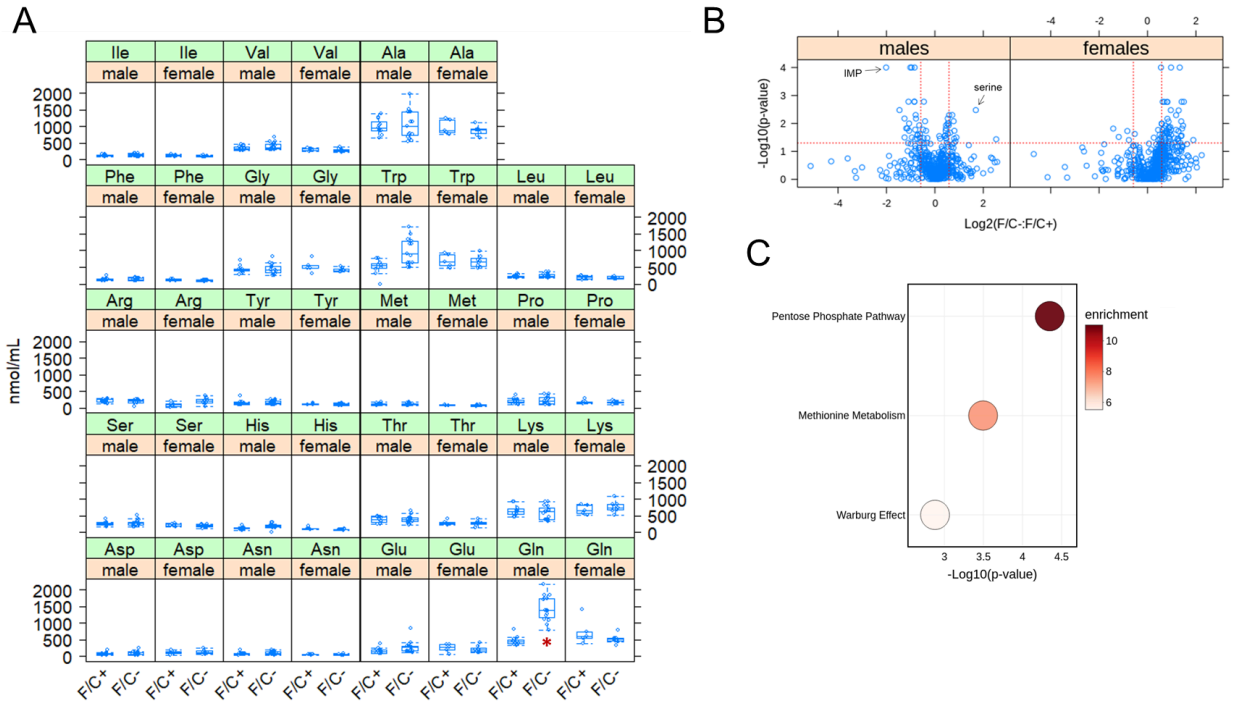

FIGURE 6. Metabolite changes in mice placed on dietary folate restriction late in life. (**A**) Steady-state serum amino acid levels were measured at 120 weeks of age using an HPLC-based assay (see Materials and Methods). The measured amounts (in nmol/mL) are on the y-axis. The different diets are on the x-axis for each amino acid, as indicated. The boxplots were drawn as in the previous figures. Differences in glutamine (Gln) levels in male mice were significant (marked with a red asterisk; p=2.6E-05, based on the Wilcoxon rank sum test). (**B**) Steady-state levels of primary and biogenic amine metabolites from liver tissue collected at 120 weeks of age were measured by GC-TOF MS and HILIC-QTOF MS/MS, respectively. Changes in the indicated pairwise comparisons were identified from the magnitude of the difference (x-axis; Log2-fold change) and statistical significance (y-axis; based on robust bootstrap ANOVA tests), as indicated by the red lines (see Materials and Methods). (**C**) Metabolite enrichment analysis based on the MetaboAnalyst platform (Chong et al., 2019) for male mice from the data in (B), for metabolites present at significantly lower levels under folate-limitation ($p<0.05$ and >1.5-fold change). The corresponding metabolic pathways are on the y-axis, and the p values are on the x-axis. The size of each bubble on the chart reflects the relative number of 'hit' metabolites in each pathway. The color of each bubble reflects the enrichment ratio, which is the number of hits within a metabolic pathway divided by the expected number of hits. Only pathways with enrichment >2 and FDR values <0.05 are shown.

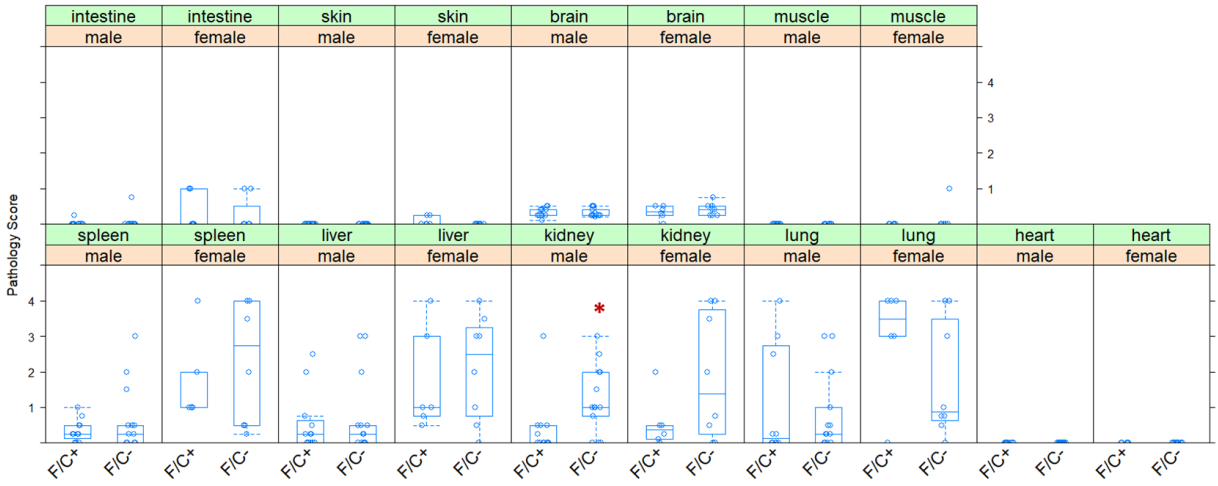

FIGURE 6 - Supplement 1. Disease load of mice placed on dietary folate restriction late in life. The pathology of the indicated tissues, collected at 120 weeks of age, was scored on a 0-4 scale (with 4 reflecting the highest degree of pathological changes; see Materials and Methods) and shown on the y-axis. The different diets are on the x-axis. Differences in kidney abnormalities in male mice were significant (indicated with a red asterisk; p=0.0165, based on the Wilcoxon rank sum test). The boxplots were drawn as in the previous figures.

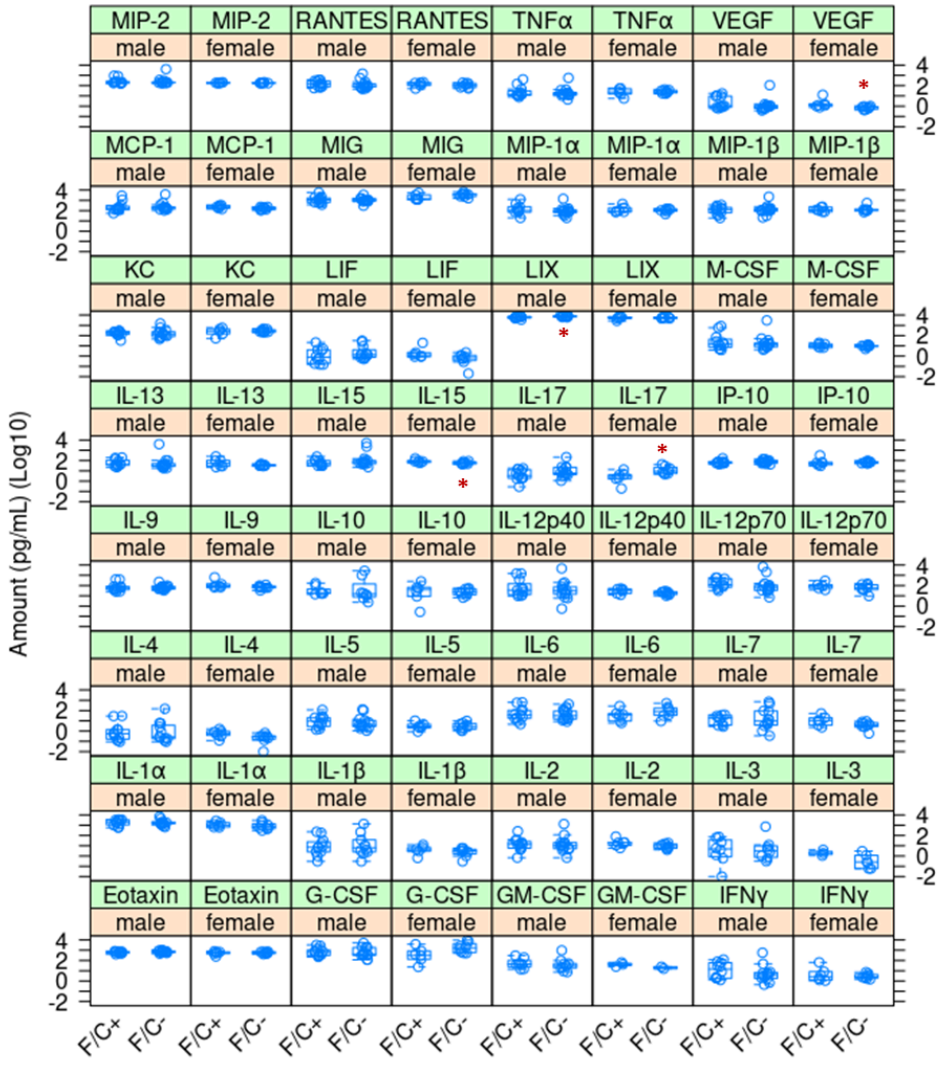

FIGURE 6 - Supplement 2. Cytokine levels of mice placed on dietary folate restriction late in life. Serum cytokine levels were measured at 120 weeks of age using a mouse multiplex cytokine assay service by Eve Technologies (see Materials and Methods). The measured amounts (in pg/mL; Log10-transformed) are on the y-axis. The different diets are on the x-axis for each cytokine, as indicated. Significant differences in the measured values within a sex and diet group are indicated with a red asterisk ($p<0.05$, based on the Wilcoxon rank sum test). The boxplots were drawn as in the previous figures.

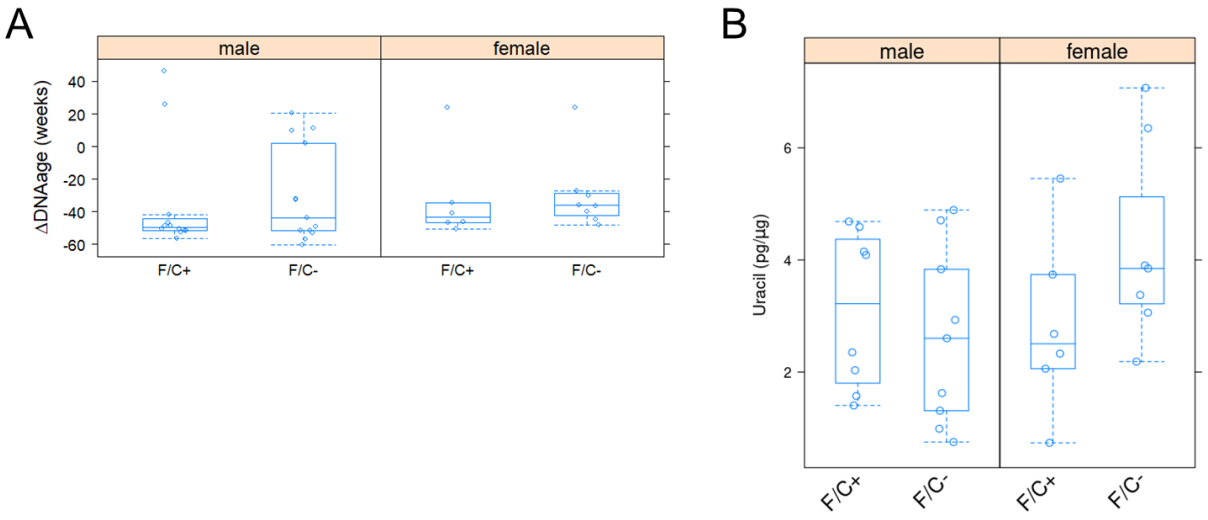

FIGURE 6 - Supplement 3. No significant changes in methylation status or uracil misincorporation in the genome of mice placed on dietary folate restriction late in life. (**A**) DNA methylation at multiple sites in the genome was measured with the epigenetic clock assay by ZymoResearch (see Materials and Methods) from liver samples at 120 weeks of age. Based on the measured against the predicted changes, a biological age estimate was compared to the actual age (ΔDNAage; shown on the y-axis). The different diets are on the x-axis. The boxplots were drawn as in the previous figures. (**B**) Uracil levels in the DNA were measured as described in Materials and Methods from liver tissue collected at 120 weeks of age (y-axis; in pg/µg). The different diets are on the x-axis. The boxplots were drawn as in the previous figures.

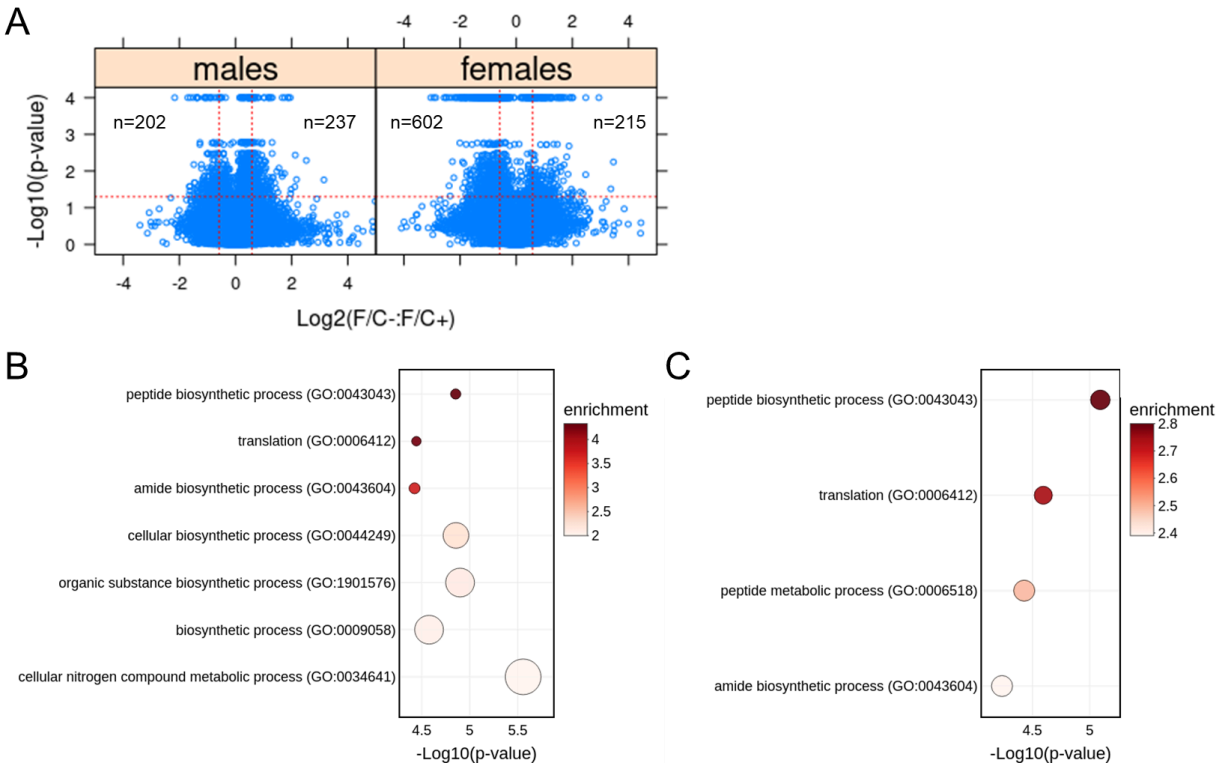

FIGURE 7. Transcriptomic changes in mice placed on dietary folate restriction late in life point to reduced protein synthesis in both sexes. (**A**) Steady-state levels of mRNAs from liver tissue collected at 120 weeks of age were measured by RNAseq. Changes in the indicated pairwise comparisons were identified from the magnitude of the difference (x-axis; Log2-fold change) and statistical significance (y-axis; based on robust bootstrap ANOVA tests), as indicated by the red lines (see Materials and Methods). The number of transcripts whose levels changed within these thresholds is shown in each case. (**B**) Transcript enrichment analysis based on the PANTHER platform (Ashburner et al., 2000; Gene Ontology Consortium et al., 2023; Thomas et al., 2022) for male mice from the data in (A), for transcripts present at significantly lower levels under folate-limitation ($p<0.05$ and >1.5-fold change) that could be assigned to a specific gene ID (n=165). The corresponding biological processes are on the y-axis, and the p values are on the x-axis. The size of each bubble on the chart reflects the relative number of 'hit' transcripts in each process. The color of each bubble reflects the enrichment ratio, which is the number of hits within a process divided by the expected number of hits. Only pathways with enrichment >2 and FDR values <0.05 are shown. (**C**) Transcript enrichment analysis for female mice from the data in (A), for transcripts present at significantly lower levels under folate-limitation ($p<0.05$ and >1.5-fold change) that could be assigned to a specific gene ID (n=490). The plots were drawn as in (B).

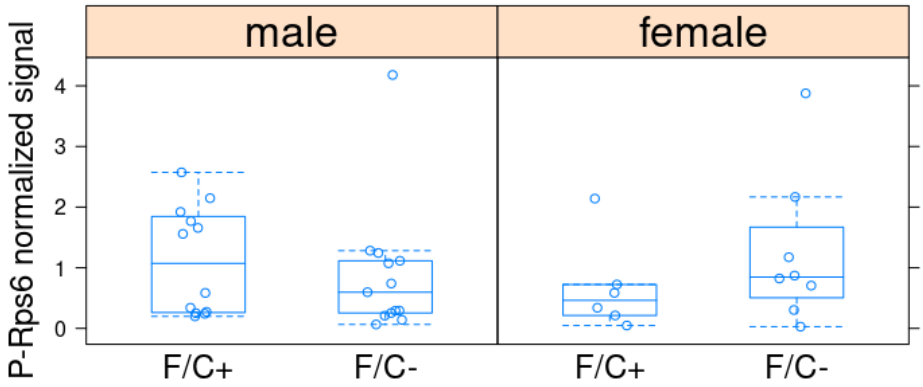

FIGURE 7 - Supplement 1. RPS6 phosphorylation levels in liver tissue are not significantly affected by dietary folate restriction late in life. Phosphorylated RPS6 (P-RPS6) levels (y-axis) were measured with a phosphospecific antibody and normalized against the signal from an antibody against RPS6 (detecting the total amount), as described in Materials and Methods. The different diets are on the x-axis. The boxplots were drawn as in the previous figures.

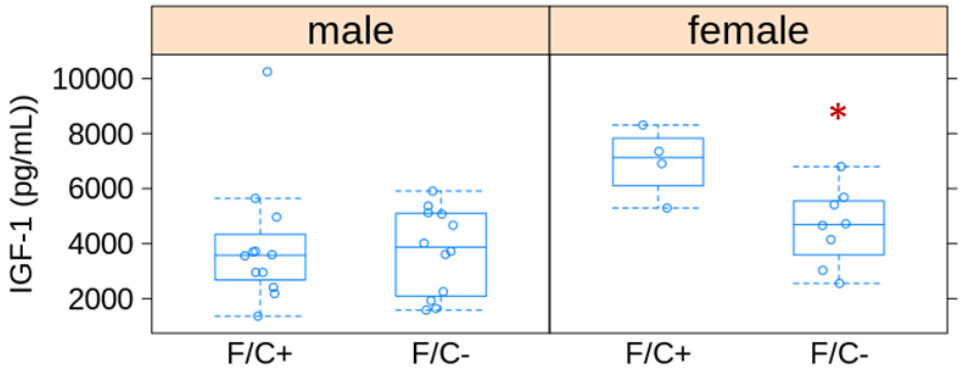

FIGURE 7 - Supplement 2. Lower IGF-1 levels in the serum of female mice placed on dietary folate restriction late in life. IGF-1 levels (in pg/mL; shown on the y-axis) were measured with a commercial mouse IGF-1 ELISA Kit (see Key Resources Table). The different diets are on the x-axis. The boxplots were drawn as in the previous figures. In female mice, the difference was statistically significant, indicated with a red asterisk (p=0.028, based on the Wilcoxon rank sum test).